University of Pardubice

Faculty of Chemical Technology

Department of Physical Chemistry

Kinetics of processes in the volume and at the surface of amorphous materials

DOCTORAL THESIS

Author: Ing. Diego Alejandro Valdés Mitchell

Supervisor: prof. Ing. Jiří Málek, DrSc.

Supervisor-Specialist: Ing. Jaroslav Barták, Ph.D.

2022

I hereby declare:

This thesis entitled *Kinetics of processes in the volume and at the surface of amorphous materials* was prepared separately. All the literary sources and the information I used in the thesis are listed in the bibliography. I got familiar with the fact that the rights and obligations arising from the Act No. 121/2000 Coll., Copyright Act, apply to my thesis, especially with the fact that the University of Pardubice has the right to enter into a license agreement for use of this thesis as a school work pursuant to § 60, Section 1 of the Copyright Act, and the fact that should this thesis be used by me or should a license be granted for the use to another entity, the University of Pardubice is authorized to claim a reasonable contribution from me to cover the costs incurred during making of the thesis, according to the circumstances up to the actual amount thereof. I am aware that my thesis will be accessible to the public in the University Library and via the Digital Library of the University of Pardubice in agreement with the article 47b of the Act No. 111/1998 Coll., on Higher Education Institutions, and on the Amendment and Supplement to some other Acts (the Higher Education Act), as subsequently amended, and with the University Pardubice's directive no. 7/2019.

In Pardubice on

I thank first of all prof. Ing. Jiří Málek, DrSc. for the opportunity I was given to work in his scientific team and for his great support during my doctoral studies.

I thank my specialist supervisor Ing. Jaroslav Barták, Ph.D. for his wise and experienced advices that were of great help to me in carrying out my scientific research.

I thank my very good friend M.Sc. Mehran Sajad and colleagues from Physical Chemistry department of University of Pardubice for their support and friendship during my doctoral studies.

I thank Cameron Quick M Chem. for giving me his professional recommendations while writing this doctoral thesis.

Big thank belong to my mother Alicia Elizabeth Mitchell Batista, my father Alejandro Antonio Valdés Lutrell, my second father Patricio Ezequiel McCarthy Graham and my girlfriend Ing. Aneta Karásková for giving me their endless support and love. Last but not least I thank my dragon boat teammates, whose energy inspired me to continue working hard to conquer my dreams.

This PhD thesis was supported by the project „Modernization of practical teaching and innovation of practical skills in technically focused study programs “, registration number CZ.02.2.67/0.0/0.0/16_016/0002458 with the financial support of the Operational Program „Research, Development and Education “. This project is co-financed by the European Union.

This thesis was also supported by the grant LM2018103 of the Ministry of Education, Youth and Sports of the Czech Republic and by the Internal Grant Agency of the University of Pardubice from year 2017 to 2021.

Annotation

The main aim of this dissertation thesis was to extend the knowledge of the crystal growth in chalcogenide glass-forming materials. Specifically, this thesis is focused on crystal growth kinetics.

The crystal growth kinetics was studied in pure selenium (*a-Se*), $Se_{95}Te_5$ system and $(GeSe_2)_x(Sb_2Se_3)_{1-x}$ pseudobinary system. This study was performed using direct (i.e. microscopy techniques – *Infrared microscopy* and *Scanning Electron Microscopy*) and indirect methods (*Differential Scanning Calorimetry, X-Ray Diffraction method, Thermomechanical Analysis*). The suitable combination of all the above-mentioned methods gave a detailed knowledge about the crystallization process in the studied materials.

Each and every experimental result was analyzed using the contemporary crystal growth theories. It is known that the crystal growth kinetics is driven by the transport of structural units through the melt-crystal interface. This transport is often described by diffusion process. Since diffusion data are often missing, they are substituted by the inverse value of viscosity according to the *Stokes-Einstein* relation (*SE*). For this reason, an exhaustive study of diffusion and viscous flow in chalcogenide glass-forming materials is also presented in this thesis.

This thesis also focused in crystal growth mechanisms occurring in different types of samples. Many of the obtained experimental outcomes of such studies were published in several scientific papers.

KEYWORDS: Chalcogenide glass, Crystal growth, Viscosity, Diffusion, Microscopy, Thermal analysis, XRD

Anotace

Hlavním cílem této disertační práce bylo rozvinout znalosti o růstu krystalů v chalkogenidových sklotvorných materiálech. Konkrétně se tato práce zaměřila na kinetiku růstu krystalů.

Kinetika růstu byla analyzována v čistém amorfním selenu (*a-Se*), v systému $Se_{95}Te_5$ a v pseudobinárním systému $(GeSe_2)_x(Sb_2Se_3)_{1-x}$. Tato studie byla provedena pomocí tzv. přímých (tj. mikroskopických metod – *Infračervená a Skenovací Elektronová mikroskopie*) a nepřímých metod (tj. *Diferenciální Skenovací Kalorimetrie, Difrakční metoda XRD, Termomechanická Analýza*). Vhodná kombinace těchto metod sloužila k získání informací o krystalizaci ve studovaných materiálech.

Každý experimentální výsledek byl analyzován podle současných teorií o růstu krystalů. Je známo, že kinetika růstu je řízena transportem strukturních jednotek z oblasti podchlazené taveniny do fáze krystalické. Tento transport lze popsat jako difúzi, avšak hodnoty difuzního koeficientu jsou pro tyto materiály velmi často nedostupné, a proto byl difúzní koeficient nahrazen inverzní viskozitou podle *Stokes-Einsteinovy rovnice* (*SE*). Z tohoto důvodu, velká část práce je věnována studii o difúzi a viskózním toku v chalkogenidových sklotvorných materiálech. Předložená práce se též věnovala studiu mechanismu růstu v různých chalkogenidových sklech. Většina získaných výsledků byla publikována v několika vědeckých časopisech.

KLÍČOVÁ SLOVA: Chalkogenidové sklo, Růst krystalů, Viskozita, Difúze, Mikroskopie, Termická Analýza, XRD

LIST OF PAPERS

Paper I

Comparison of Lateral crystal Growth in Selenium Thin Films and Surface of Bulk Samples
J. Barták, D. Valdés, J. Málek, V. Podzemná, S. Slang and K. Pálka
Cryst. Growth Des. **18** (2018), 4103 – 4110

Paper II

Relationship between Crystal Growth and Surface/Volume Mobilities in $Se_{95}Te_5$ Bulk Samples and Thin Films
S. Martinková, D. Valdés, S. Slang, K. Pálka, J. Barták
Acta Mater. **213** (2021), 116953

Paper III

Analysis of Viscosity Data in As_2Se_3, Se and $Se_{95}Te_5$ Chalcogenide Melts Using the Pressure Assisted Melt Filling Technique
J. Barták, P. Koštál, D. Valdés, J. Málek, T. Wieduwilt, J. Kobelke, M. A. Schmidt
J.Non Cryst. Solids **511** (2019), 100 – 108

Paper IV

Crystal Growth in Ge-Sb-Se Glass and its Relation to Viscosity and Surface Diffusion
D. Valdés, S. Martinková, J. Málek, J. Barták
J. Non Cryst. Solids **566** (2021), 120865

Paper V

Combination of Indirect and Direct Approaches to the Description of Complex Crystallization Behavior in $GeSe_2$-rich Region of Pseudobinary $GeSe_2$-Sb_2Se_3 system
P. Honcová, D. Valdés, J. Barták, J. Málek, P. Pilný, S. Slang
J. Non Cryst. Solids **568** (2021), 120968

Paper VI – Draft

Study on Crystal Growth in $(GeSe_2)_x(Sb_2Se_3)_{1-x}$ (x = 0.6 – 0.9) Glass-Forming Materials
D.Valdés, S. Martinková, P. Koštál, J. Barták

Table of contents

SYMBOLS

A	Preexponential factor in Friedmann´s equation
A'	Condensation parameter
a_0	Interatomic distance
A_{EV}	Evaporation parameter
a_H	Hole volume
B	Constant of the two-dimensional (2D) surface nucleated growth model
$B_{Surface}$	Surface diffusion parameter
B_{VFT}	Empirical constant of VFT equation
C	Concentration of diffusing particles
C_{2D}	Constant of the two-dimensional (2D) surface nucleated growth model
C_{MYEGA}	MYEGA constant
C_{Volume}	Volume diffusion parameter
D	Diffusion coefficient
d	Sample thickness
D_G	Diffusion coefficient of vapor molecules in an inert atmosphere
D_S	Surface diffusion coefficient
D_u	Diffusion coefficient of the rate-controlling species in the melt
D_V	Volume diffusion coefficient
E_A	Activation energy of the overall nucleation-crystal growth process
E_G	Crystal growth activation energy
E_N	Nucleation activation energy
F	Applied force to the sample during viscosity measurements
f	Number of active sites in the crystalline phase
$F(T)$	Thermodynamic driving force of crystal growth
F_{Visc}	Viscous flow
H	Enthalpy
h	Grating amplitude
h_0	Initial grating amplitude
h_{pen}	Penetration depth for viscosity measurements
H_R	Hruby´s coefficient

K	Decay constant
k	Shape parameter of the reaction order model (RO)
k_B	Boltzmann constant
K_{MYEGA}	MYEGA constant
Krate	Rate constant
L	Filling length
l	Crystal length size
m	Nucleation and crystal growth parameter in JMA model
M	Kinetic parameter of Šesták-Berggren model
$m_{Fragility}$	Fragility
M_r	Molecular weight
N	Kinetic parameter of Šesták-Berggren model
N_t	Number of tracer atoms per unit area
p	Nucleation JMA parameter
P	Applied pressure during PAMFT
q	Cooling rate
q_{JMA}	Crystal-dimension parameter in JMA model
r	Nucleum size
R	Universal gas constant
r^*	Nucleum critical size
R_C	Capillary radius
r_{ind}	Indenter radius
r_L	Lateral distance
t	Time
T	Temperature
T_0	VFT constant
T_{12}	Viscosity glass transition temperature
T_g	Glass-Transition temperature
T_m	Melting point
u	Crystal growth rate
u_{kin}	Kinetic term of crystal growth
U_R	Reduced growth rate
u_S	Surface crystal growth rate

V	Volume
v	Number of molecules at the surface per unit area
W^*	Thermodynamic barrier to form a nuclei during homogeneous nucleation
$W^{*,Het}$	Thermodynamic barrier to form a nuclei during heterogeneous nucleation
W^{*Max}	Maximal value of W*
x	Penetration depth of tracer atoms
z	Surface profile of hole
α	Degree of crystallization
β_{DSC}	Heating rate
β_S	Stretch parameter
γ	Surface tension
ΔC_p	Difference of the isobaric heat capacity
ΔG	Gibbs free energy difference between the crystalline and amorphous phase
ΔG_V	Free energy difference between the melt and the crystalline phase
ΔH_C	Enthalpy of crystallization
ΔH_m	Enthalpy of melting
ΔS_m	Entropy of melting
ΔT	Undercooling
η	Viscosity
η_0	VFT constant
θ	Contact angle
λ	Grating period
ρ_0	Vapor pressure at equilibrium
σ	Surface tension between the gas phase and the nuclei
σ_i	Surface tension between the surface impurity and the forming nuclei
σ_{int}	Interfacial free energy between the nucleus and the amorphous phase
σ_s	Surface tension between the surface and the gas phase
ϕ	Correcting factor between W^* and $W^{*,Het}$
Ω	Molecular volume

ABBREVIATIONS

2D	Two-dimensional crystal growth model
AC	Autocatalytic Model
AFM	Atomic Force Microscope
CD	Compact Disk
CNT	Classical Nucleation Theory
DSC	Differential Scanning Calorimetry
DTA	Differential Thermal Analysis
DVD	Digital Versatile Disk
GC	Glass-Crystal Mode
GFA	Glass Forming Ability
HT	High Temperature
IR	Infrared Microscopy
JMA	Johnson-Mehl-Avrami model
LT	Low Temperature
MYEGA	Mauro-Yue-Ellison-Gupta-Allan equation
NG	Normal growth model
OM	Optical Microscopy
PAMFT	Pressure Assisted Melt Filling Technique
PCM	Phase-changing materials
RO	Reaction Order model
SDG	Screw-dislocation growth model
SE	Stokes-Einstein equation
SEM	Scanning Electron Microscopy
TA	Thermal Analysis
TMA	Thermomechanical analysis
VFT	Vogel-Fulcher-Tammann
XRD	X-Ray diffraction

INTRODUCTION

Through the past years, chalcogenide glass-forming materials have been an important asset in the development of diverse applications and technologies [1-3]. For this reason, a deep characterization of these materials is given within this thesis, within a focal point on the study of the crystal growth kinetics. The crystallization process is a phenomenon directly utilized for some technological devices, as is the case of data storage in phase-changing materials [4-6]. In other cases, the crystallization process affects the quality of certain technological devices [7]. Understanding the crystallization process in these materials allows not only optimization of existing technologies, but also the development of new technological devices. Although the crystallization process has been at the center of attention among the scientific community for many decades, there are still several discrepancies between the current crystal growth theories and the real crystal growth process occurring in glass-forming materials. To obtain a deeper knowledge about the crystal growth in the studied materials, several experimental techniques were applied. Crystallization can be observed directly or indirectly. Indirect study of the crystallization kinetics is possible because during crystal growth a change in several properties such as: enthalpy, volume, or electric conductivity, occurs. Among the most prevalent experimental techniques for measuring such properties are: Differential Scanning Calorimetry (*DSC*) and Differential Thermal Analysis (*DTA*). Both methods are very useful for the calculation of important parameters such as the change of enthalpy ΔH of the studied kinetic process or the melting point T_m of the studied material. These methods give information about the overall nucleation-growth process as is published in the literature [8-11]. However, these methods do not give a complete information about the crystal growth mechanism. To study the crystal growth mechanism, several microscopic techniques such as: Optical Microscopy (*OM*), Infrared Microscopy (*IM*) and Scanning Electron Microscopy (*SEM*) are used. Some other complementary techniques give indispensable information about the structural (X-Ray Diffraction (*XRD*)) and mechanical properties (Thermomechanical Analysis (*TMA*)) of the studied materials.

CHAPTER I: GLASS

Since ancient times, glass has been present in the development of humankind. Apart from its decorative uses glassy materials have been a convenient ally in the development of many technologies. Chalcogenide glasses in particular have been a center of big interest among the scientific community during the last decades. Due to their exceptional properties, they are a crucial material during the development and fabrication of new technological devices. To fabricate high-quality technological devices, it is paramount to characterize the behavior of these materials under certain conditions. One of the primary phenomena that can affect the properties of glassy materials is crystallization. The crystal growth process has both positive and negative effects on the quality of such technological devices.

Synthesis of glasses

The synthesis of glass-forming materials is presented in *Figure 1*, where a temperature dependence of the volume V and enthalpy H is shown. Here it is seen that when a melt is cooled down slowly through its melting point T_m, a significant decrease in material´s properties (V, H) is observed. This is influenced by the crystallization process, which starts at temperatures below T_m. As temperature continues decreasing, so does the volume of the crystal, however, this volume decrease is not as notable as the volume decrease of the solidifying melt. This is due to the expansion coefficient differences between both melt and crystal [12]. Since the structural particles had enough time to arrange into a periodical structure (i.e., crystalline phase), the material is in equilibrium.

In order to avoid the crystallization process, it is necessary to cool down the melt rapidly (i.e. the cooling rate q is a key factor during the synthesis of glass, as is shown in *Figure 1* $q^1>q^2$) [13]. By cooling the melt rapidly, as is presented in *Figure 1*, the volume and enthalpy of the material continue decreasing unceasingly until the glass transition temperature T_g is reached. At lower temperatures the viscosity of the material rises, and the mobility of structural units (atoms, molecules) becomes lower and lower. Then, the crystallization process becomes less and less feasible [12, 14, 15].

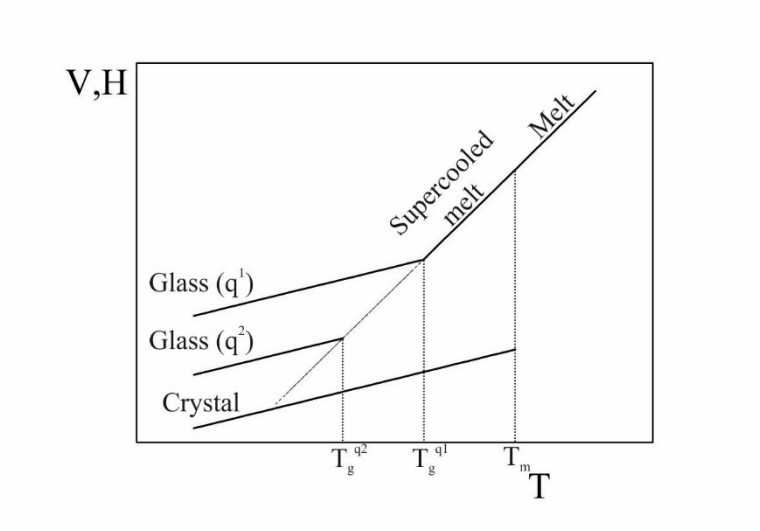

Figure 1 Temperature dependence of volume (V) or enthalpy (H) of a glass-forming material

Glass structure

Glasses are defined as non-crystalline materials characterized by the absence of long-distance periodicity in their atomic structure [16]. A deeper explanation of the atomic arrangement in glasses was presented by Zachariasen [17], where it was stated that the atomic structure of a glass is not entirely disordered, but there are not two atoms structurally similar as is shown in *Figure 2*. On the other hand, crystalline materials are considered from the view of thermodynamics as stable materials, which have a well-ordered structure at short, medium, and long range (i.e. atoms are arranged into a periodic matrix) as is shown in *Figure 2* [16, 18].

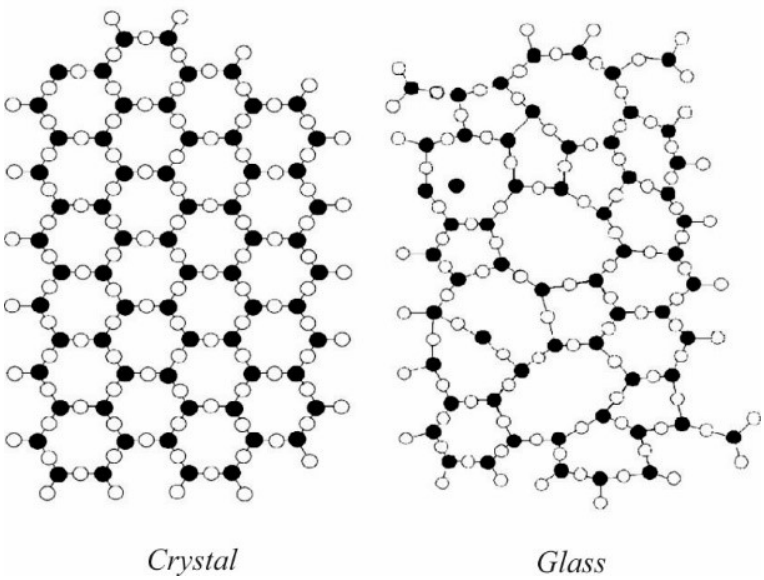

Figure 2 Structural differences between crystal and glass [19]

Thermal properties of glass-forming materials

Knowledge of thermal properties allows understanding of the behavior of glass-forming materials in dependence on temperature. One of the most important thermal properties of these materials is the *Glass Forming Ability (GFA)*, which can be estimated by the so-called Hrubý coefficient H_R [20]:

$$H_R = \frac{T_c - T_g}{T_m - T_c} \quad (1)$$

As it is clear from *Eq.1*, H_R is dependent on thermal parameters such as crystallization temperature (T_c), T_g and T_m. According to Hrubý [20], when the crystallization process takes place close to the T_g region (i.e. T_c-T_g term has a low value) then forming a glass is very difficult for these materials. On the other hand, if the T_m-T_c term has a low value it means that the crystallization process takes place close to T_m (i.e., these materials form glasses very easily). By calculating *GFA*, it is possible to estimate the thermal stability of glass-forming materials, which is highly affected by T_g.

Chalcogenide glass-forming materials

These non-oxide, non-crystalline materials are composed of elements of the 16. group of the periodic table. (Sulfur, Selenium, and Tellurium). Due to their outstanding properties, chalcogenide glasses are important materials for the development of new technologies such as: potentiometric sensors [21, 22], optoelectronic applications [23, 24], phase changing materials (*PCM*) [6, 25, 26], and solar cells [2]. For this reason, understanding their behavior at different conditions is a topic of attentiveness. For example, in the case of *PCM* such as: *DVD*, *CD*, etc.; the data is recorded via glass-to-crystal transformation or vice versa. On the other hand, there are several technological devices [7, 27] where crystallization should be avoided. Considering the importance of understanding the crystallization behavior to the fabrication of new technologies, a deep analysis of the crystal growth mechanism in chalcogenide-based glassy materials is presented in this thesis. Specifically, in *Se*, *Se-Te* and *Ge-Sb-Se* glass-forming materials.

Se

Amorphous selenium is major asset ally in the production of low photo flux imaging applications [28], medical drugs [29-33], photosensors [34, 35], batteries [36, 37], solar cells [38] among other things [39-41]. Since pure selenium finds its application in several

technological devices, a proper characterization of such materials has been at the center of attention among the scientific community for many decades already. Recently, a significant study on physical aging of selenium glass-forming materials was performed by Kumar Pal et al. [42].

Selenium gives the impression of a simple element, but it has astonishing properties and a complex molecular arrangement [43]. Mikla et al.[44] presented a study on the molecular structure of selenium. Along with the molecular arrangement in a selenium chain, two types of segments were found. A "chain-like" segment conformed by trigonal *Se* and a "ring-like" segment formed by Se_8 molecules. This molecular arrangement is shown in *Figure 3*.

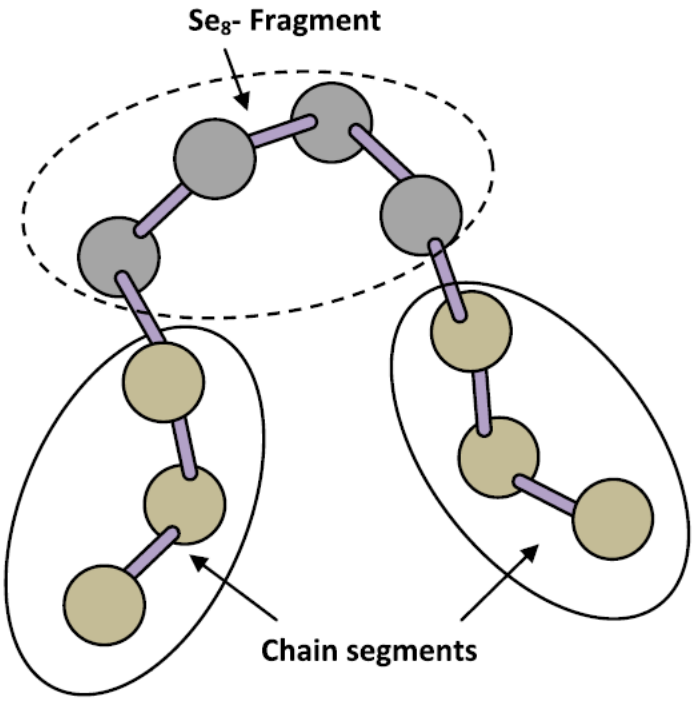

Figure 3 Molecular arrangement in a Selenium chain [44]

Some other studies on crystal growth in selenium glass-forming materials were performed previously [45-47]. However, this doctoral thesis presents the very first comparison between the crystal growth in thin films, at the surface of bulk and in the volume of bulk selenium samples.

Se-Te

Due to their outstanding properties, both Tellurium (*Te*) and Selenium (*Se*) are used in the fabrication of several technologies (solar cells, optical storage, optical fibers) [48-52]. However, Tellurium-based materials are characterized by a low *GFA*, as is shown in

Figure 4. The thermal stability of such materials is increased with increasing content of *Se* as was presented by Svoboda et al. [53]. Apart from *GFA*, it was found that a suitable combination of both elements improves the physico-chemical properties of these materials [54]. Studies on electric properties of such materials proved that increasing content of *Se* increases the photoconductivity [55] and electrical conductivity [56].

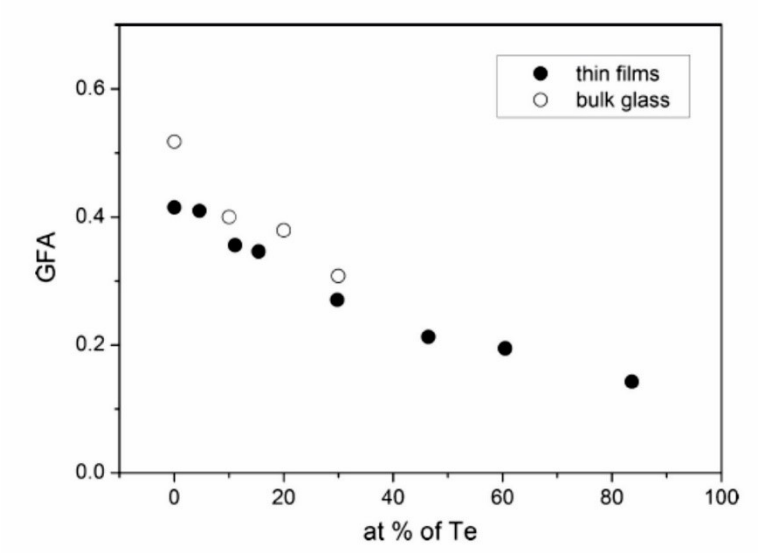

Figure 4 GFA of Se-Te glass-forming materials [53]

A computer simulation performed by Mauro and Varshneya [57], proposed a very close approximation of structural arrangement in *Se-Te* glass-forming materials. *Se-Te* system is formed by randomly integrated *Te* atoms into the *Se* chain as is shown in *Figure 5*.

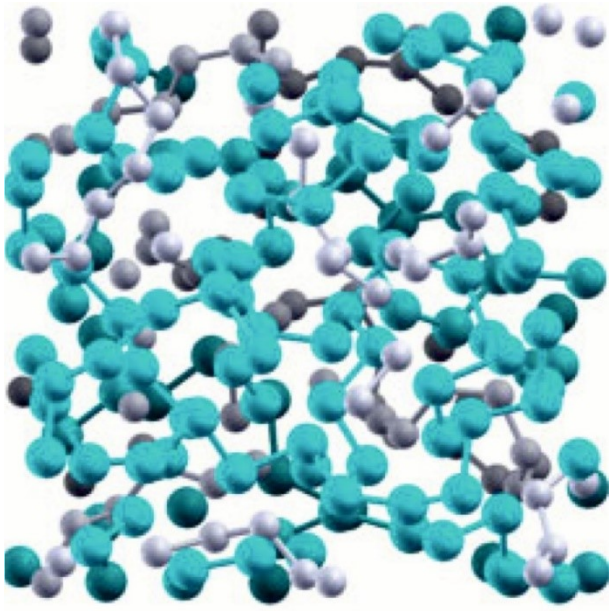

Figure 5 Se-Te glass structure-Se atoms (grey atoms), Te (blue atoms)[57]

Over the last decades, several studies on this system have been performed. Specifically, on the crystal growth [58-60]. Nevertheless, a deeper study of the crystal growth in *Se-Te* is presented in this thesis. Concretely, the relationship between the crystal growth and mobilities along the surface and in the volume of $Se_{95}Te_5$ samples is explored.

Ge-Sb-Se

Materials of this system are very promising glass-forming materials with a wide range of technological applications [61-65]. In the last few decades, many studies on the structural and thermal characterization of this system have been performed [66-68]. Since glass-forming chalcogenide materials like *Se* show a considerable thermal instability and short lifetime, a suitable combination of *Ge*, *Sb* and *Se*, increases the *GFA,* which elevates the thermal stability and lifetime needed for technological applications [69, 70]. *GFA* of this system was studied by many authors [71, 72].

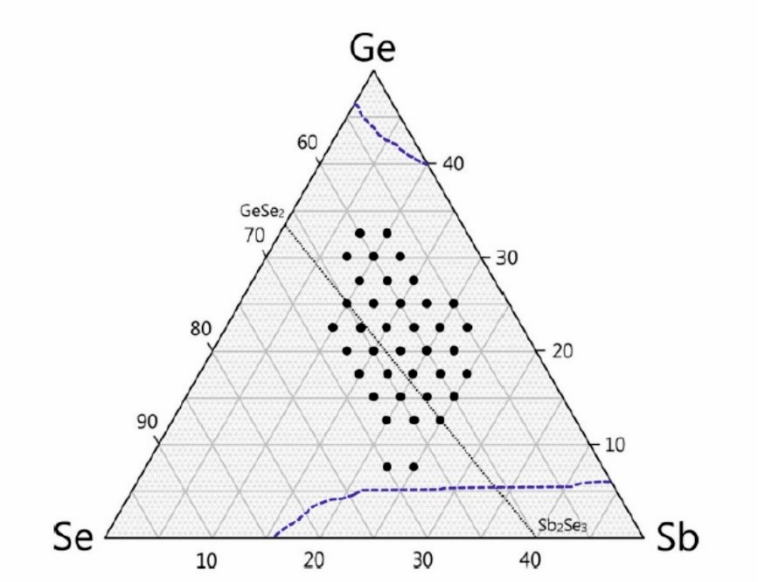

Figure 6 Glass-forming ability region of Ge-Sb-Se materials [71]

Figure 6 is a phase diagram presented by Lee et al. [71], where the dark dots represent the compositions, for which thermal expansion coefficient was measured. Dotted lines show *GFA* region of these glass-forming materials and the straight line corresponds to a pseudobinary system, which divides the *Ge-Sb-Se* system into two parts: $GeSe_2$-Sb_2Se_3-*Se* and *Ge-*$GeSe_2$-Sb_2Se3-*Sb* [73]. According to Bordas and Clavaguera [73], in *Ge-Sb-Se* system, various constituent binary systems such as: *Sb-Se*, *Ge-Se* and *Ge-Sb* can be formed. However, Sb_2Se_3 and $GeSe_2$ are the only compounds of this system, which present a congruent melting.

In the case of $GeSe_2$, it is known, that multiple crystalline phases with structural differences are formed. These crystalline structures are known as: High Temperature *(HT)-$GeSe_2$* and Low Temperature *(LT)-$GeSe_2$* [74, 75]. Generally, germanium dichalcogenides have a linear chain structure [75], which in the case of *HT-$GeSe_2$* is formed by corner-sharing connections and edge-sharing connections [74-76]. On the other hand, *LT-$GeSe_2$* structure is formed by corner-sharing connections only [74-76]. The structural arrangement of both *HT-$GeSe_2$* and *LT-$GeSe_2$* was presented by Nakaoka et al. [76] and is shown in *Figure 7*.

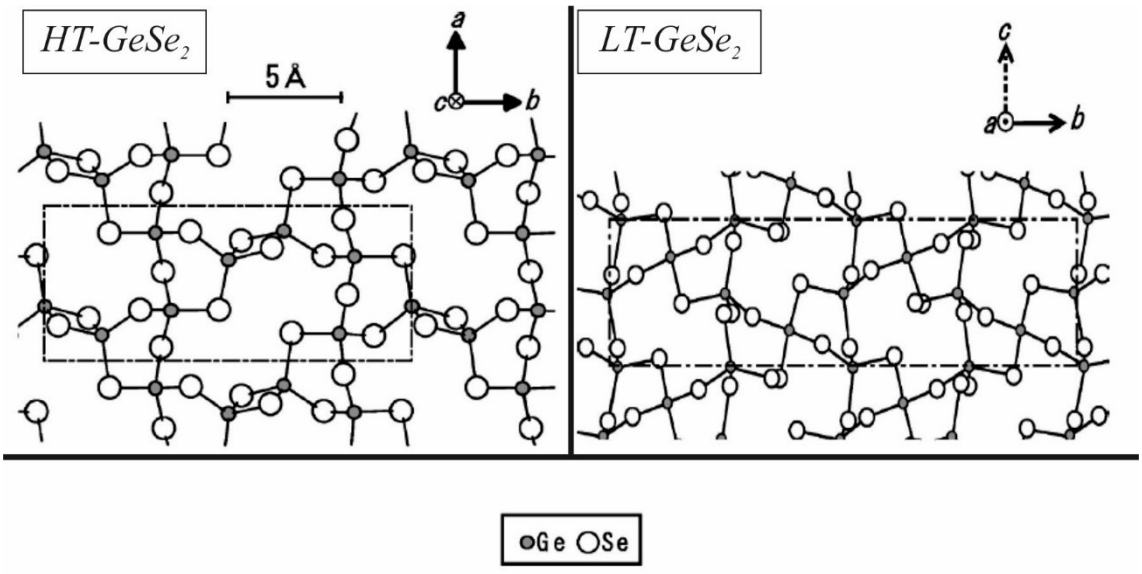

Figure 7 Structural differences between HT-$GeSe_2$ and LT-$GeSe_2$ crystalline phases [76]

According to studies performed previously [77-79], in the crystalline structure of Sb_2Se_3 every *Sb(1)* atom is coordinated by 2 *Se(1)*, 3 *Se(2)* and 1 *Se(3)* atoms, which form a distorted octahedron. On the other hand, *Sb(2)* atoms are coordinated by 3 *Se(1)*, 2 *Se(2),* and 2 *Se(3)* atoms. This structural arrangement is shown in *Figure 8*.

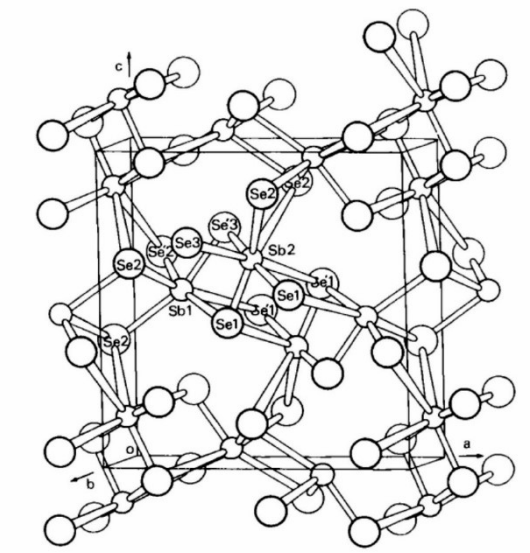

Figure 8 Sb_2Se_3 crystalline structure [77]

Since *Ge-Sb-Se* alloys are very important materials, over the years several studies on their characterization have been performed; specifically on the crystallization [8, 10]. In this thesis an intensive analysis of the crystal growth mechanism in *Ge-Sb-Se* samples is presented.

CHAPTER II: CRYSTALLIZATION

Crystallization can be defined as the transformation from non-ordered glassy state to ordered crystalline state. This process is composed of two elemental steps: nucleation and crystal growth. During nucleation, structural precursors (nuclei) are formed. Additional incorporation of structural units to the stable nucleus results in crystal growth. Detailed information about both processes is presented within the following text.

Nucleation

The nucleation process is described by the classical nucleation theory (*CNT*). This theory assumes that between two individual phases separated by an interphase of zero thickness, a thermodynamic equilibrium exists. *CNT* expresses the formation of stable clusters (i.e. the crystal growth can occur only on these clusters) with critical size r^* (i.e. supercritical cluster) [80].

Nucleation can be homogeneous or heterogeneous. The differences between both types of nucleation lie in the probability of cluster formation along the material. In the case of the homogeneous nucleation, the clusters form with the same probability (homogeneously) in every part of the sample. On the other hand, during the heterogeneous nucleation clusters are formed mostly in specific places such as dislocations or surface defects. This is because at these places the thermodynamic barrier that controls the nucleation process is smaller than the thermodynamic barrier for the homogeneous nucleation [80-82].

Homogeneous nucleation

According to *CNT*, the nucleation process is a casual process dependent on thermodynamics [81]. The thermodynamic barrier W^* needed to form nuclei with a spherical shape during homogeneous nucleation corresponds to the change of the Gibbs free energy and is expressed by the following equation:

$$W^* = 4\pi r^2 \sigma_{int} - \frac{4}{3}\pi r^3 \Delta G_V \qquad (2)$$

r represents the size of the nucleus, σ_{int} is the interfacial free energy between the forming nucleus and the amorphous phase and ΔG_V represents the free energy difference between the melt and crystalline phase [80, 83, 84].

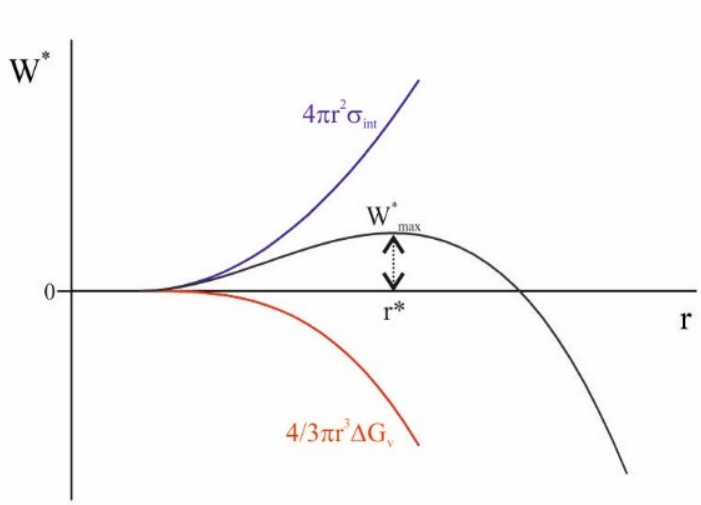

Figure 9 Change of the free Gibbs energy (W^*) with the formation of nuclei of size r during homogeneous nucleation.

As mentioned previously, crystal growth process takes place only on stable nuclei with critical size r^*. At this point as is shown in *Figure 9,* W^* reaches maximal value W^*_{max}. From *Eq. 2*, it is possible to calculate r^* by assuming that the nuclei are formed as spherical particles [80, 82]:

$$\frac{\delta W^*}{\delta r} = 8\pi r\sigma_{int} - 4\pi r^2 \Delta G_V = 0 \tag{3}$$

$$r^* = \frac{2\sigma_{int}}{\Delta G_V} \tag{4}$$

Then by combining *Eq.2* with *Eq. 4*, W^*_{max} is obtained:

$$W^*_{max} = \frac{16}{3}\pi \frac{\sigma^3_{int}}{\Delta G^2_V} \tag{5}$$

Heterogeneous nucleation

From the thermodynamic point of view as was mentioned previously, heterogeneous nucleation is characterized by a lower thermodynamic barrier than W^*. This is due to the decrease of surface energy, which is affected by the presence of impurities or structural defects in the material. The thermodynamic barrier for the formation of supercritical nuclei during heterogeneous nucleation ($W^{*,Het}$) is expressed by:

$$W^{*,Het} = W^* \cdot \phi \tag{6}$$

where ϕ is a correcting factor, which acquires values from 0 to 1. This factor is directly proportional to the contact angle (θ) between the supercooled liquid and a certain surface, which

in this case could be an impurity or a structural disorder. This proportion is expressed by the following relation [85]:

$$\phi(\theta) = \frac{1}{4} \cdot (1 - \cos\theta)^2 \cdot (2 + \cos\theta) \tag{7}$$

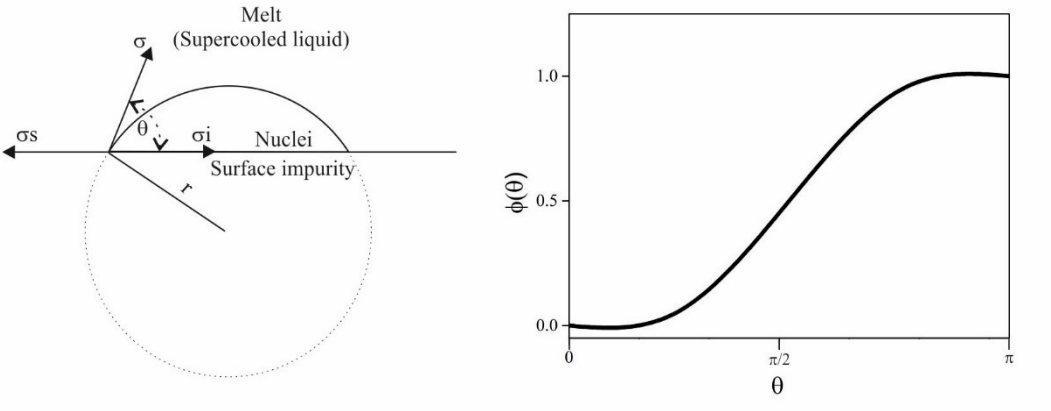

Figure 10 Interaction between supercooled liquid and surface impurity during heterogeneous nucleation.

Figure 10 represents the steady state of the interaction between a supercooled liquid and a surface impurity. σ_s corresponds to the surface tension between the surface and the gas phase, σ is the surface tension between the gas phase and the nuclei (cluster) and σ_i represents the surface tension between the surface impurity and the forming nuclei.

Crystal growth

The crystal growth analysis is necessary to understand the crystal growth mechanism in glass-forming materials. According to previous studies on the crystal growth in chalcogenide glass-forming materials, there are several discrepancies between the studied phenomena and the current crystal growth framework. Along the following paragraphs, deeper information on this topic will be given.

Kirkpatrick in his work [86] stated that the crystal growth rate *u(T)* can be driven by three factors: flow of latent heat away from the growing crystalline surface, reactions at the crystal-melt interface and diffusion in the melt (long-range or short-range).

In the case that *u(T)* is ruled by the long-range diffusion in the melt, Christian [87] expressed *u* of a flat interface by the equation:

$$u = k \cdot \left(\frac{D}{t}\right)^{1/2} \tag{8}$$

k corresponds to a constant involving concentration terms, *D* is the diffusion coefficient of the rate-controlling species present in the melt and *t* represents the time. Then, according to *Eq. 8* if a crystal size vs. the square root of *t* plot is made, it will show a linear trend.

In the case that the growth rate controlling process is the short-range diffusion close to the crystal-melt interface, the crystal growth rate finds its steady state. Thus, the crystal growth is independent of time (i.e. the crystal size is linearly dependent on time) [88].

When the crystal growth rate is controlled by the flow of the latent heat from the crystal-melt interface, the interphase has a cellular structure [89] and similarly like in the above-mentioned case, the crystal growth rate is normally independent of time. The effect of the latent heat flow at the crystal-melt interphase was studied by Hooper and Uhlmann [90]. For small undercooling values, it was determined that if the latent heat is produced at a higher rate than is removed, then the temperature at the interphase will raise until the growth rate is slower, so the latent heat is removed at the same rate as is produced. Consequently, the crystal growth rate is ruled by the reaction at the crystal-melt interphase. Then, in the case of a homogenous system the crystal growth rate is independent of position and subsequently independent of time. In such a case, crystal size vs. time plots show straight lines. This is the case for the crystal growth in chalcogenide glass-forming materials. As is verified in this thesis, crystal size vs. time plots are straight lines and their slopes correspond to the crystal growth rate (see Chapter V – Experimental Part).

Crystal growth kinetics

The crystal growth rate is dependent on two individual factors (i.e., kinetic term and thermodynamic term). The kinetic term $u_{kin}(T)$ is related to the mobility of structural units through the liquid-crystal interface. On the other hand, the thermodynamic term *F(T)* represents the energetic barrier that has to be overpassed to enable the crystal growth. Then the crystal growth rate *u(T)* is expressed by the equation:

$$u(T) = u_{kin}(T) \cdot F(T) \tag{9}$$

$$u_{kin}(T) \propto D(T) \propto \eta(T)^{-1} \tag{10}$$

From *Eq. 10*, it is evident that $u_{kin}(T)$ is proportional to the diffusion coefficient *D(T)*. The study of the diffusion process in glass-forming materials is key to understand the crystal growth mechanism. Generally, for chalcogenide glass-forming materials *D(T)* data are often missing.

Due to this fact, the Stokes-Einstein equation (*SE*) is usually used to substitute the *D(T)* with a physical parameter that is more easily measurable, the viscosity η. *SE* states that the diffusion coefficient is proportional to the reciprocal value of viscosity (*Eq. 10*).

However in some cases the *SE* relation is found lacking and it is necessary to calculate a correcting parameter ξ, that represents the extension of decoupling between *D(T)* and η*(T)* [91, 92].

$$u_{kin}(T) \propto \eta(T)^{-\xi} \tag{11}$$

The decoupling of u_{kin} and η is observed only on several types of samples. For example, the crystal growth mechanism in the volume of a sample is linked with the viscous flow of the studied material. Then ξ finds its value close to 1, which means that the kinetic part of the crystal growth rate can be substituted by η according to *SE*. On the other hand, for crystal growth in thin films and at the surface of bulk samples the mechanism is different. In our previous research on the crystal growth in chalcogenide glasses, a strong decoupling of *SE* is observed [47, 60, 93]. This reveals that the crystal growth kinetics in such samples is not influenced by the viscous flow, but by the surface diffusion. Further details on this topic will be discussed later on.

Crystal growth models

Since the measurement of the crystal growth and subsequent calculation of the crystal growth rate *u(T)* for a wide temperature range is not always possible using microscopic techniques, crystal growth models are used. These crystal growth models are: Normal growth model (*NG*), Screw-dislocation growth model (*SDG*) and the 2D-surface nucleated growth model [86, 94].

Normal crystal growth (NG)

This model is based on the assumption that the liquid-crystal interface is atomically rough and that allows structural precursors to attach to any active site along with the forming crystalline phase [86, 94-96], as is shown in *Figure 11*.

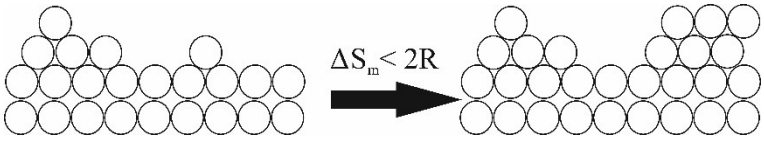

Figure 11 Normal crystal growth mechanism

$$u(T) = f \cdot \frac{k_B \cdot T}{3 \cdot \pi \cdot a_0^2 \cdot \eta} \cdot \left[1 - exp\left(-\frac{\Delta G}{R \cdot T}\right)\right] \quad (12)$$

The temperature dependence of crystal growth rate can be expressed by *Eq. 12* [86, 92]. Where ΔS_m is the melting entropy, a_0 is the interatomic distance, k_B corresponds to the Boltzmann constant, R is the universal gas constant, ΔG is the change of Gibbs free energy between the undercooled melt and the crystalline phase and f represents the number of active sites in the crystalline phase, where the structural units can attach. In this case, f is equal to 1 [86, 92].

Screw dislocation growth (SDG)

The screw dislocation growth model is based on the expectation that crystals grow in specific places of the sample, forming a screw-like structure [96, 97] as is shown in *Figure 12*.

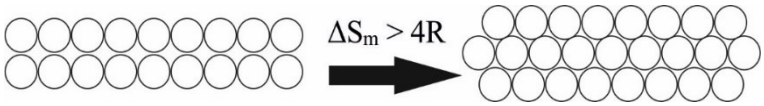

Figure 12 Screw dislocation growth mechanism.

This growth model can be expressed by *Eq. 12* [86, 94] and the parameter f can be expressed as:

$$f \cong \frac{\Delta T}{2\pi \cdot T_m} \quad (13)$$

where ΔT is the undercooling ($\Delta T = T_m - T$) and T_m is the melting temperature. The crystal growth in materials, which have a high value of melting entropy ($\Delta S_m > 4R$) is expected to behave according to this mechanism [92, 95].

Two-dimensional (2D) surface nucleated growth

This model assumes that structural units coming from the amorphous phase can attach at the edges of a rough crystalline layer enabling a lateral growth [86, 98, 99]. Crystal growth rate is expressed by *Eq. 14.*

$$u(T) = \frac{C_{2D}}{\eta} exp\left(-\frac{B}{T\Delta T}\right) \quad (14)$$

where C_{2D} and B are empirical parameters.

Reduced crystal growth rate U_R

The reduced crystal growth rate U_R is a very important tool to estimate the appropriate growth model describing the crystal growth mechanism. According to Jackson, Uhlmann and Hunt [98] the crystal growth is dependent on ΔT of the system among the interface. This interaction can be expressed by:

$$U_R = \frac{u \cdot \eta}{1 - exp\left(-\frac{\Delta G}{R \cdot T}\right)} \tag{15}$$

According to this equation an U_R vs. ΔT plot (*Figure 13*) can be constructed for each crystal growth model (normal growth, screw dislocation and 2D-surface nucleated model). As stated in *Eq. 12* for the normal crystal growth model, U_R is independent of ΔT, then the U_R vs. ΔT plot is disclosed as a permanent horizontal line. As stated in *Eqs.12* and *13* for screw dislocation growth model, U_R is linearly proportional to ΔT, then the U_R vs. ΔT dependence describes a straight line with a positive slope. In the case of 2D-surface nucleated model, U_R is exponentially dependent on ΔT as is shown in *Eq.14*. Then in the U_R vs. ΔT plot a curve with an exponential behavior is expected.

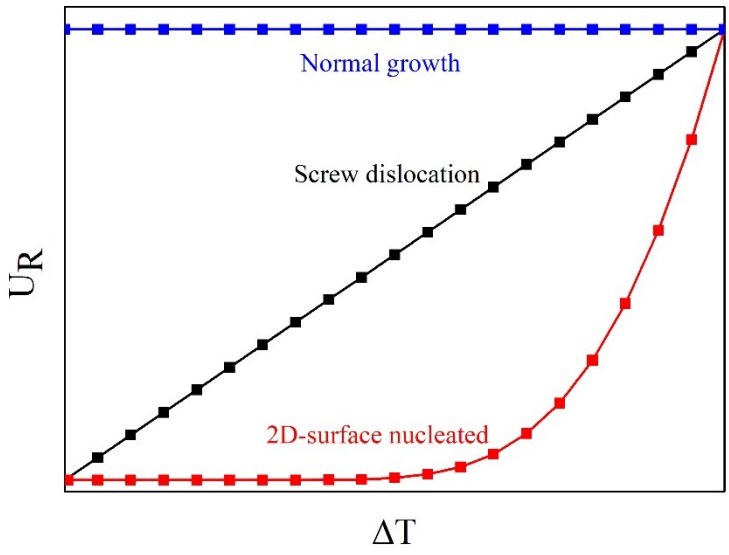

Figure 13 Reduced crystal growth U_R dependence on undercooling ΔT

Thermodynamics of crystal growth

The thermodynamic driving force of crystal growth is expressed by the equation:

$$F(T) = 1 - exp\left(-\frac{\Delta G}{R \cdot T}\right) \tag{16}$$

where ΔG represents the change of the Gibbs free energy between the crystalline and amorphous phase, R is the universal gas constant and T is the temperature [86]. ΔG is a function of temperature and can be expressed using the difference of the isobaric heat capacity ΔC_P between the crystalline and the amorphous phase [100].

$$\Delta G = \Delta H_m \frac{\Delta T}{T_m} - \int_T^{T_m} \Delta C_p(T) dT + T \int_T^{T_m} \frac{\Delta C_p(T)}{T} dT \quad (17)$$

where ΔH_m is the enthalpy of melting. Due to the complexity of measurement of ΔC_p among the crystallization region in the case of chalcogenide-based materials, the heat capacity data is frequently missing. Therefore, for estimating ΔG, several approximations were proposed by Thompson and Spaepen [101], Singh and Holz [102] and Hoffman [103]. However, the most appropriate and widely applied is the Turnbull approximation [104]:

$$\Delta G = \Delta H_m \frac{\Delta T}{T_m} \quad (18)$$

Barták et al. [59] showed, that even the simple approximation of ΔG proposed by Turnbull (*Eq. 18*) is appropriate for the crystal growth models calculations. As the attention in ΔG approximations is focused on the crystal growth, then it is assumed that ΔH_m can be substituted by ΔH_c (the enthalpy of crystallization), especially for systems with a very complex melting process.

Crystal growth followed by thermal analysis

Methods of thermal analysis monitor the changes of physical properties of the analyzed material along with a temperature program. These methods can be performed under isothermal and non-isothermal conditions. During isothermal measurements it is possible to observe the changes of the monitored property with time. On the other hand, at non-isothermal conditions the monitored property changes in dependence on temperature.

In contrast to microscopic techniques, methods of thermal analysis (*TA*) usually provide information about the overall nucleation-crystal growth process. The most used thermal analysis techniques are: *Differential Scanning Calorimetry (DSC)* and *Differential thermal analysis (DTA)*.

The output signal of *DSC* is the heat flow Φ, which is related to the crystallization rate expressed as a change of degree of crystallization α in time t ($d\alpha/dt$) as is shown in the relation:

$$\Phi = \Delta H \left(\frac{d\alpha}{dt}\right) \quad (19)$$

ΔH represents the enthalpy change during the followed process. The crystallization kinetics are dependent on the temperature and on the crystal growth mechanism. Then, the crystallization rate ($d\alpha/dt$) is calculated by the equation:

$$\frac{d\alpha}{dt} = K_{rate}(T) \cdot f(\alpha) \quad (20)$$

f(α) is a conversion function. $K_{rate}(T)$ represents the rate constant, which is dependent on the temperature. The temperature dependence of this rate constant is expressed by the well-known Arrhenius equation:

$$K_{rate}(T) = A \cdot exp\left(-\frac{E}{RT}\right) \quad (21)$$

A is a pre-exponential factor and *E* corresponds to the activation energy.

f(α) function is related to the crystal growth mechanism, which can be described by several growth models. The most known models are:

- *Johnson-Mehl-Avrami (JMA)*
- *Diffusion model*
- *Šesták-Berggren model*
- *Reaction order model (RO)*

Johnson-Mehl-Avrami (JMA) model

According to this model, *f(α)* function can be calculated by the equation:

$$f(\alpha) = m(1-\alpha)[-\ln(1-\alpha)]^{1-\frac{1}{m}} \quad (22)$$

parameter *m* represents both nucleation and crystal growth and is expressed as $m=p + q_{JMA}$. If homogeneous nucleation is assumed ($p=1$), then $m=1+q_{JMA}$. Parameter q_{JMA} describes the dimensions of the crystal (*Figure 14*) and assumes values from 1 to 3 [105-107].

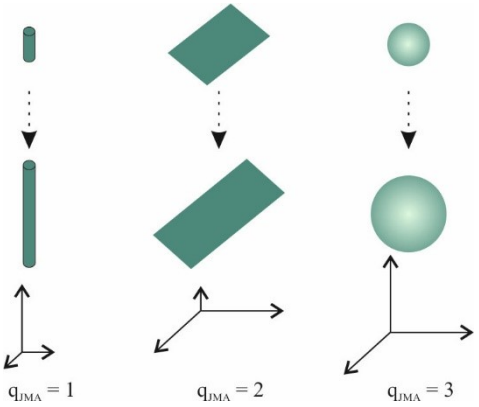

Figure 14 Dimensional changes in the parameter q of the JMA model

Diffusion model

This model was proposed to describe a reaction between a gas and a solid substance, where the diffusion is responsible for the reaction mechanism. Specifically, for reacting systems, where the reactants and the products have distinct compositions [108].

Šesták-Berggren model

This two-parametric (*M, N*) model also known as autocatalytic (*AC*) is used to describe complex kinetic processes even though its parameters are physically meaningless. For this model, the function *f(α)* is expressed by the relation [108]:

$$f(\alpha) = \alpha^M (1-\alpha)^N \tag{23}$$

Reaction order model (RO)

The formulation of this model assumes that the free energy of the nucleation process is comparable with the crystal growth free energy or when the formation of nuclei among the studied material is anisotropic. The *f(α)* function is possible to express as:

$$f(\alpha) = (1-\alpha)^k \tag{24}$$

parameter *k* expresses the shape of the formed nuclei. If the nuclei have a spherical-like structure, then *k = 1/3.* In the case of cylindrical nuclei parameter *k* is equal to *1/2* [109].

Choosing the most suitable model is the key to properly describe and understand the crystal growth kinetics in glassy materials. To do so, Málek [110] proposed a very skillful method, where he proposed to choose the best kinetic model by calculating two functions *y(α)*

and *z(α)*. If the kinetic study is performed at isothermal conditions, then both functions are calculated by the following equations:

$$y(\alpha) = \Phi \tag{25}$$

$$z(\alpha) = \Phi \cdot t \tag{26}$$

In the case of non-isothermal conditions, then:

$$y(\alpha) = \Phi \cdot exp\left(-\frac{E_A}{RT}\right) \tag{27}$$

$$z(\propto) = \Phi \cdot T^2 \tag{28}$$

where E_A is the crystallization activation energy. In the case of chalcogenide glasses, the kinetics of crystallization is often described by the *JMA* or the Šesták-Berggren model.

Activation energy of crystal growth

The definition of the activation energy is an important parameter during the analysis of crystal growth kinetics. The activation energy of crystal growth can be calculated from different experimental data, such as:

- DSC data
- Crystal growth rate data (obtained via microscopic techniques)

Calculation of the activation energy from DSC data

In the case of DSC measurements, the activation energy of the overall crystallization process (E_A) can be calculated from isothermal and non-isothermal data using different methods such as: Kissinger method [111, 112], Ozawa method [113] and Friedman method [114].

Kissinger method

Kissinger method allows calculation of E_A from non-isothermal data. The maximum of a *DSC* peak is reached at the temperature T_p. This method assumes that at the maximum of the *DSC* peak the reaction rate is at its maximum and the conversion degree (α) remains constant at every heating rate β_{DSC}. The position of the *DSC* peak is linked to the heating rate β_{DSC}, then by measuring several *DSC* curves at different β_{DSC}, it is possible to calculate E_A using the following equation:

$$\frac{d\ln\left(\frac{\beta_{DSC}}{T_p^2}\right)}{d\left(\frac{1}{T_p}\right)} = -\frac{E_A}{R} \tag{29}$$

Ozawa method

This method is also used to calculate the activation energy of crystallization at non-isothermal conditions. Similarly, as in the Kissinger method, E_A is calculated from the knowledge of β_{DSC} and T_p as is shown in the following equation:

$$\ln \beta_{DSC} = -1.0516\frac{E_A}{RT_p} + const \tag{30}$$

Friedman (isoconversional) method

Using this method, it is possible to calculate E_A from the knowledge of heat flow Φ_α and temperature T_α at a certain conversion degree. It is then possible to calculate the activation energy from both isothermal and non-isothermal data using the following equation:

$$\ln \Phi_\alpha = [\Delta H \cdot A \cdot f(\alpha)] - \frac{E_A}{R} \cdot \frac{1}{T_\alpha} \tag{31}$$

It is important to mention that E_A corresponds to the overall nucleation crystal growth process. Yinnon and Uhlmann [107] proposed a relation between the nucleation (E_N) and crystal growth (E_G) activation energy. This relation is shown in *Eq. 32*:

$$E_A \approx \frac{E_N + q_{JMA} \cdot E_G}{m} \tag{32}$$

This equation *(Eq.32)* is related to the type of nucleation as is shown in *Eq. 22*

Calculation of the activation energy from crystal growth rate data obtained from microscopy technique

With the knowledge of the crystal growth rate data, the crystal growth activation energy E_G can be calculated using the Arrhenius relation in a short temperature range, where its temperature dependence is expressed by the linearized Arrhenius relation:

$$\ln u = \ln u_0 - \frac{E_G}{R \cdot T} \tag{33}$$

u is the crystal growth rate obtained from microscopy measurements, u_0 is a preexponential factor and T represents the temperature.

CHAPTER III: DIFFUSION IN SOLID STATE

Since the kinetics of crystal growth is dependent on the diffusion of structural units through the liquid-crystal interface, it is crucial to understand the diffusion mechanism in glass-forming materials. A deeper description of the diffusion mechanism in glassy materials will be discussed in the following text.

Comparison between the surface and volume mobility in glass-forming materials

As it has been mentioned before, the crystal growth mechanism is strongly related to the mobility of structural units through the liquid-crystal interface. Based on literature [115, 116], it is suitable to state that the mobility dynamics in an amorphous material at the surface is different from the dynamics towards the volume. Particles at the surface are strained only from the inner part of the material. This leads to higher mobility of these structural units along the surface, like the lateral crystal growth observed e.g., by Barták et al. [47]. In some cases, the mobility of these structural units is so high that they keep mobile even below T_g. This phenomenon was observed in polymer [115-119], organic [120, 121], chalcogenide [122] and metallic [123, 124] glasses. At temperatures above T_g, no differences between the mobility dynamics at the surface and in the volume are observed [119]. Zhang and Yu [125] presented a study in polymer glasses, which revealed that at temperatures above T_g, the mobility dynamics at the surface and in the volume of the bulk is driven by the viscous flow. However, at temperatures below T_g, the mobility along the volume of the bulk becomes slower and subsequently the growth mechanism is ruled by the fast surface diffusion [126]. Selfsame behavior was observed in organic glasses [120, 121, 127]. Previous research concluded in the fact that understanding the real meaning of the glass transition temperature, will provide a better understanding of the surface mobility dynamics in glassy materials. To do so, it would be suitable to not just determine a unique T_g, but the changes in T_g according to the place where crystallization takes place in the sample [118].

On the other hand, the mobility of the structural units in the volume of glassy materials is affected by the collaborative diffusion of neighboring particles. As can be observed in the following *Figures 15-17*. Currently, in the case of volume diffusion, several diffusion mechanisms are known. Between the most probable mechanisms belong vacancy diffusion, interstitial diffusion and interstitialcy diffusion.

Vacancy diffusion mechanism

The simplest mechanism is vacancy diffusion, where a particle can diffuse just towards a vacancy in the opposite direction [128]. This mechanism is shown in *Figure 15.*

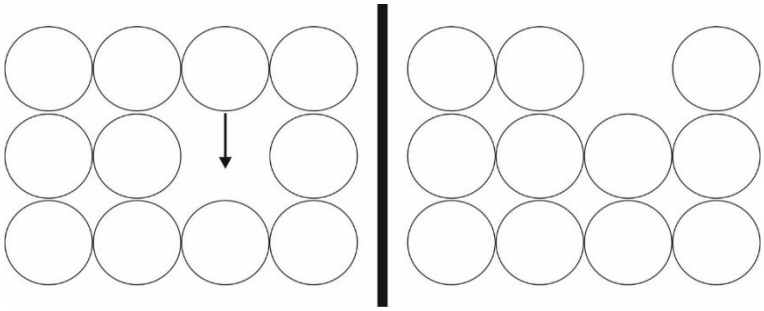

Figure 15 Vacancy diffusion

Interstitial diffusion mechanism

In the case of the interstitial diffusion mechanism shown in *Figure 16*, the particles move along interstitial spaces in the lattice [128].

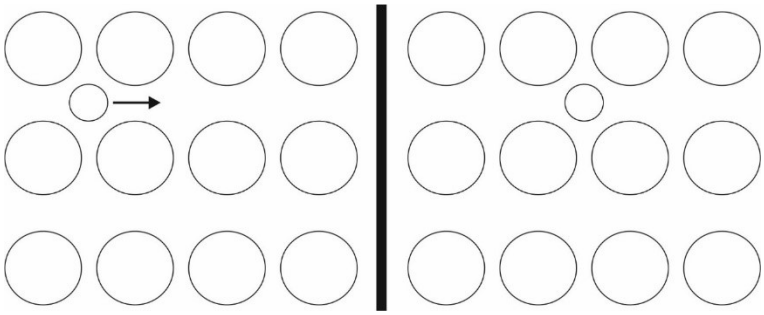

Figure 16 Interstitial diffusion

Interstitialcy diffusion mechanism

Another mechanism is the interstitialcy diffusion and occurs when an interstitial ion or particle moves onto a regular site of the lattice shoving a particle from its original place to an interstitial site [128].

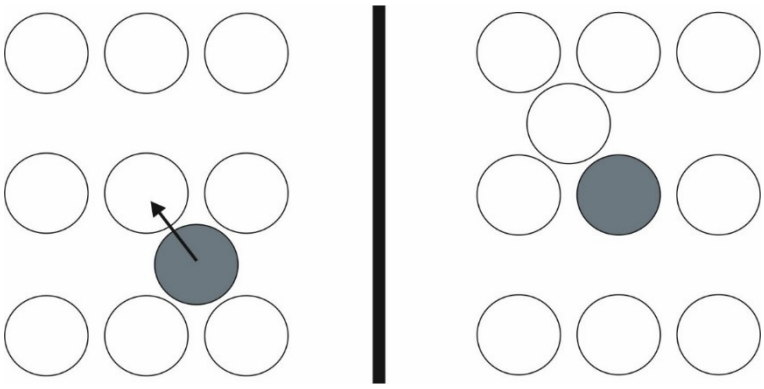

Figure 17 Interstitialcy diffusion

The diffusion mechanisms shown above mainly take place in the volume of the analyzed materials [128].

Measurement of diffusion in glassy materials

Radiotracer method

A tracer particle or atom is deposited at the surface of the studied solid. Then at isothermal conditions, the concentration of tracer particles in different sections of the matrix after a certain period is measured. These tracer particles are characterized by their radioactivity. This technique belongs to the most frequent techniques to study the diffusion process in solids [129]. According to the Fick's second law, the diffusion of particles in glass-forming materials can be expressed by the equation:

$$\frac{\partial C}{\partial t} = D \cdot \frac{\partial^2 C}{\partial x^2} \tag{34}$$

where *C (x,t)* represents the concentration of diffusing particles at a certain location (*x*) in a certain time (*t*) and *D* is the diffusion coefficient [130, 131]. During these experiments, the concentration of tracer atoms is measured by sectioning the analyzed material in several parts as is shown in *Figure 18.*

For this method then, it is necessary to express the Fick´s second law solution for thin films by the equation [129, 131]:

$$C(x,t) = \frac{N_t}{\sqrt{\pi \cdot D^* \cdot t}} \cdot exp\left(-\frac{x^2}{4 \cdot D^* \cdot t}\right) \tag{35}$$

where *x* is the distance, which the tracer atom penetrates the analyzed material. *N* represents the number of tracer atoms deposited per unit area, *D** is the diffusion coefficient of the tracer atom and *t* is the time.

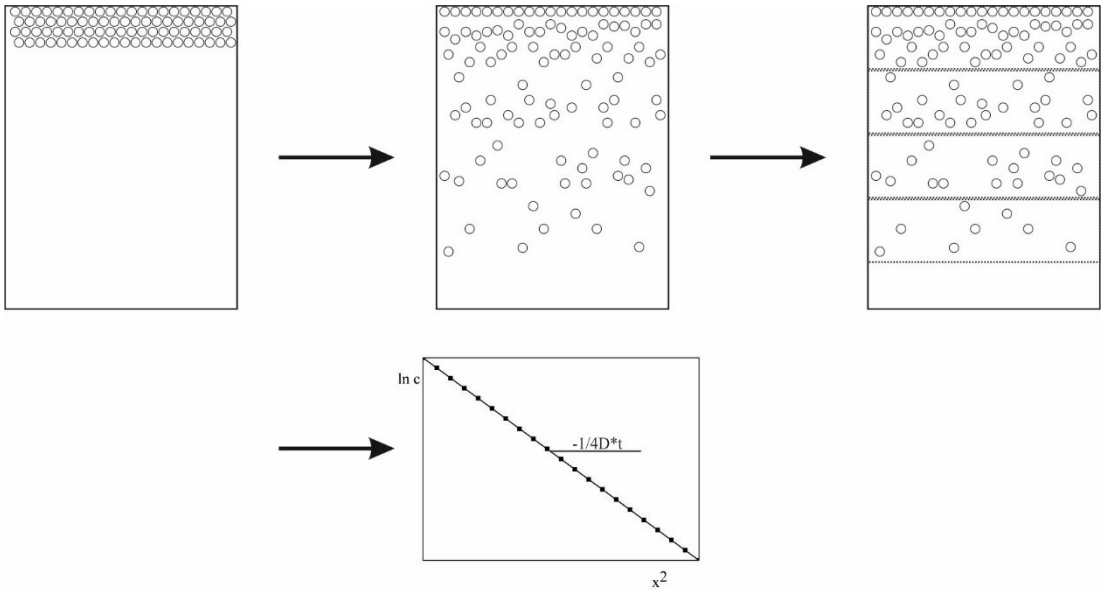

Figure 18 Radiotracer method for calculating the diffusion coefficient in solid state.

This technique is used concretely to study the diffusion of particles towards the core of the studied material.

Study of Surface Self-Diffusion

Mullins [132] presented a method, where the smoothing of a surface structure is followed using an *Atomic Force Microscope* (*AFM*). If the analyzed surface has a single-period sinusoidal shape, then the change of grating amplitude *h* exponentially decreases with time as is shown in *Figure 19* and the decrease can be expressed by the equation:

$$h = h_0 \cdot exp \cdot \left[-(K \cdot t)^{\beta s}\right] \tag{36}$$

where h_0 is the grating amplitude at the beginning of the measurement, *K* represents the decay constant and β_S corresponds to the stretch parameter, which takes a value close to 1.

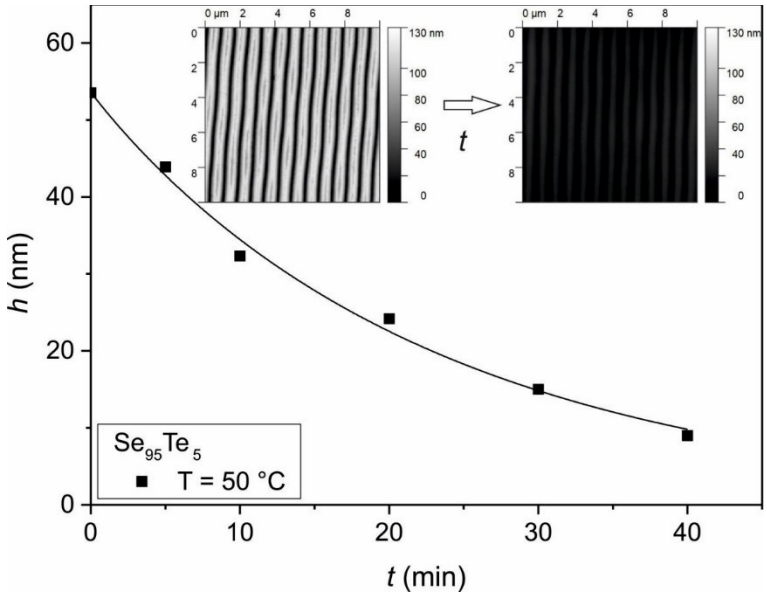

Figure 19 Measurement of the grating amplitude (h) at the surface of $Se_{95}Te_5$ glass in time (t) by AFM [122]

Mullins [132] stated that the smoothing of a surface is affected by transport processes of viscous flow (F_{Visc}), evaporation-condensation process (A_{EV} and A' respectively), volume diffusion (C_{Volume}) and surface diffusion ($B_{Surface}$). Then, the constant K is expressed by the relation:

$$K = F_{Visc} \cdot \frac{2 \cdot \pi}{\lambda} + A_{EV} \cdot \left(\frac{2 \cdot \pi}{\lambda}\right)^2 + \left(A' + C_{Volume}\right) \cdot \left(\frac{2 \cdot \pi}{\lambda}\right)^3 + B_{Surface} \cdot \left(\frac{2 \cdot \pi}{\lambda}\right)^4 \quad (37)$$

λ corresponds to the grating period. The terms of *Eq. 37* are expressed by the following equations:

$$F_{Visc} = \frac{\gamma}{2 \cdot \eta} \quad (38)$$

$$A_{EV} = \frac{p_0 \cdot \gamma \cdot \Omega^2}{(2 \cdot \pi \cdot M_r)^{1/2} \cdot (k_B \cdot T)^{3/2}} \quad (39)$$

$$A' + C_{Volume} = \frac{\rho_0 \cdot D_G \cdot \gamma \cdot \Omega^2}{k_B \cdot T} + \frac{D_V \cdot \gamma \cdot \Omega}{k_B \cdot T} \quad (40)$$

$$B_{Surface} = \frac{D_S \gamma \Omega^2 v}{k_B T} \quad (41)$$

where γ represents the surface tension, η corresponds to the viscosity, p_0 is vapor pressure at equilibrium, Ω is the molecular volume of the analyzed material, M_r represents the molecular weight, ρ_0 defines the equilibrium vapor density, v is the number of molecules at the surface per unit area and D_G, D_V and D_S are diffusion coefficients that describe the diffusion of vapor molecules in an inert atmosphere, the volume self-diffusion, and the surface diffusion,

respectively. In the case that volume self-diffusion and the evaporation-condensation process are neglected, then *Eq. 37* is modified to the form:

$$K = F_{Visc} \cdot \frac{2 \cdot \pi}{\lambda} + B_{Surface} \cdot \left(\frac{2 \cdot \pi}{\lambda}\right)^4 \tag{42}$$

If the decay of the surface is driven by diffusion, then K is expressed by:

$$K \approx B_{Surface} \cdot \left(\frac{2 \cdot \pi}{\lambda}\right)^4 \tag{43}$$

On the other hand, if the decay is driven by the viscous flow, then K is equal to:

$$K \approx F_{Visc} \cdot \frac{2 \cdot \pi}{\lambda} \tag{44}$$

Mullins [132] proposed another method to study the surface decay in the case that the surface does not present a sinusoidal profile. In this case, the surface mobility is studied by measuring the profile of a small perturbance or nanohole (*Figure 20*). The surface profile z of a hole as a function of t and the lateral distance r_L from the center to the edge of the hole is studied. If the surface decay is driven by the surface diffusion, then z is expressed by the equation:

$$z(r_L, t) = \frac{a_H}{8\pi \left(B_{Surface} \cdot t\right)^{1/2}} \sum_{n=0}^{\infty} \left[(-1)^n \frac{\Gamma\left(\frac{n+1}{2}\right)}{2^{2n}(n!)^2} \left(\frac{r_L}{\left(B_{Surface} \cdot t\right)^{1/4}} \right)^{2n} \right] \tag{45}$$

where a_H represents the volume of the studied hole. On the other hand, if the surface decay is driven by the viscous flow, then $z(r_L,t)$ is expressed as:

$$z(r_L, t) = \frac{a}{2\pi (F_{Visc} t)^2 \left(1 + \frac{r_L}{F_{Visc} t}\right)^{3/2}} \tag{46}$$

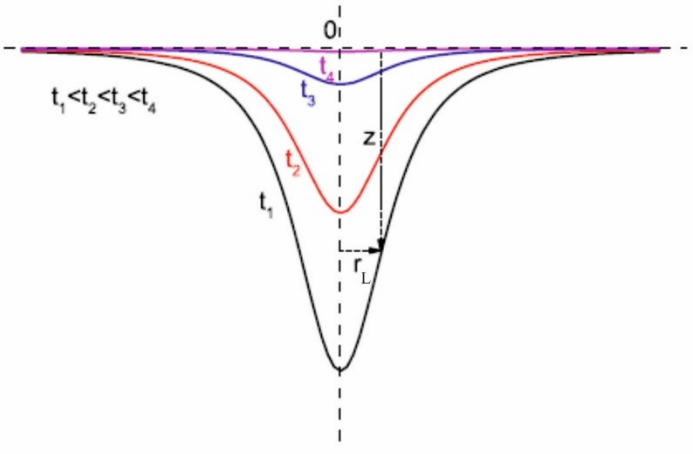

Figure 20 Change of a hole profile in dependence of time at a constant temperature [133]

The estimation of diffusion coefficients in chalcogenide glass-forming materials gives a deeper grasp on the crystal growth mechanism. However, currently the study of diffusion in these materials is in an underdeveloped stage, and diffusion coefficient data are often missing. Nevertheless, diffusion coefficient can be replaced by viscosity using the so-called Stokes-Einstein (*SE*) equation. *SE* states that the diffusion coefficient is proportional to the reciprocal value of viscosity ($D \sim \eta^{-1}$). For this reason, a deeper attention on the viscosity is given in the following chapter.

CHAPTER IV:
VISCOSITY

The viscosity is an important parameter during the analysis of kinetic processes in glassy materials. Thanks to the viscosity, it is possible to understand the behavior of the abovementioned materials in a wide temperature range, which is indispensable during their fabrication and manipulation. Since this work is focused on the study of crystal growth in chalcogenide glasses, viscosity is an important ally during the kinetic analysis of the different crystal growth mechanisms in several types of samples. The knowledge of the temperature dependence of viscosity allows us to obtain several key parameters for the characterization of glassy materials such as: fragility ($m_{Fragility}$), viscosity glass transition temperature (T_{12}), parameters of structural relaxation, etc. In this chapter a detailed explanation of the experimental methods used to measure the viscosity and its temperature dependence is given. Nowadays, as it was summarized by Koštál et al. [134], various techniques are used to measure the viscosity in glass-forming materials in different temperature regions (glass-undercooled melt-melt). However, in this thesis the viscous behavior was studied using the methods mentioned as follows.

Viscosity measurement in glassy materials

For measurement of viscosity in the undercooled melt region, viscosity behavior is analyzed using a Thermomechanical Analyzer (*TMA*). This measurement is possible to carry out using several experimental setups, which are suitable to calculate the viscosity in a certain temperature region. The typical measuring methods are:

- Penetration method
    - Cylindrical indenter
    - Hemispherical indenter
- Parallel-plate method

Penetration methods

As is obvious from the name of this experimental technique, the viscosity is measured by penetrating the analyzed sample with different types of indenters (cylindrical or hemispherical) applying a constant force *F*, as is shown in *Figure 21.*

Cylindrical indenter

The penetration method using cylindrical indenter is shown in *Figure 21(A)*. For this experimental arrangement, the viscosity η is calculated by the equation [135]:

$$\eta = \frac{F}{8 \cdot r_{ind} \cdot \left({}^{dh_{pen}}/_{dt} \right)} \tag{47}$$

Where r_{ind} is the radius of the cylindrical indenter, h_{pen} answers the penetration depth into the analyzed sample and t represents the penetration time. Based on previous experiments this experimental technique is suitable for measuring viscosity in the range of 10^{10} to $10^{7,5}$ Pa.s [136].

Hemispherical indenter

As is shown in *Figure 21(B)*, this measuring technique penetrates the analyzed sample with a hemispherical-like indenter applying a constant force F. For this experimental setup the viscosity η is expressed by the equation [137, 138]:

$$\eta = \frac{9}{32\sqrt{2 \cdot r_{ind}}} \cdot \frac{F \cdot t}{{}^{3}/_{2}\, h_{pen}} \tag{48}$$

In comparison with the penetration method using a cylindrical indenter, this method allows the measurement of high viscosity values ($10^{13.5}$ to $10^{7.5}$ Pa.s) [134, 136, 139].

Both penetration methods give very adequate results. However, there are several issues that may affect the quality of the measurement. Recently, the most important issues were mentioned by Koštál et al. [134]. First, this method requires long time to reach a stable penetration rate into the sample. The effect of the penetration rate is particularly noticeable at high viscosity values. In the case of the penetration method with a hemispherical indenter, *Eq. 48* is obtained from the assumption that h_{pen} is shorter than r_{ind}. Last but not least, it is important to mention that for both penetration methods (i.e., with cylindrical and hemispherical indenters), the sample should be large enough to avoid the so-called edge effect.

Parallel-plate method

In this experimental method the analyzed sample is placed between two corundum parallel plates. Then, both plates apply a constant force that squeezes the analyzed sample

(*Figure 21(C)*). In this method the viscosity is calculated using the following equation specified for a cylindrical-like sample [140, 141]:

$$\eta = \frac{2 \cdot \pi \cdot F \cdot d^5}{3 \cdot V \cdot \left(^{dd}/_{dt}\right) \cdot (2 \cdot \pi \cdot d^3 + V)} \tag{49}$$

where *d* is the thickness and *V* is the volume of the analyzed sample. The volume of the sample can be calculated from the initial size of the cylindrical-like sample and from the knowledge of the thermal expansion of the studied sample[142]. This method is suitable to measure the viscosity in the region of 10^4 to 10^{10} Pa.s [134, 140]. Koštál et al. [134], mentioned that this method can be affected by specific (i.e. slip and stick) conditions at the sample-plate interface.

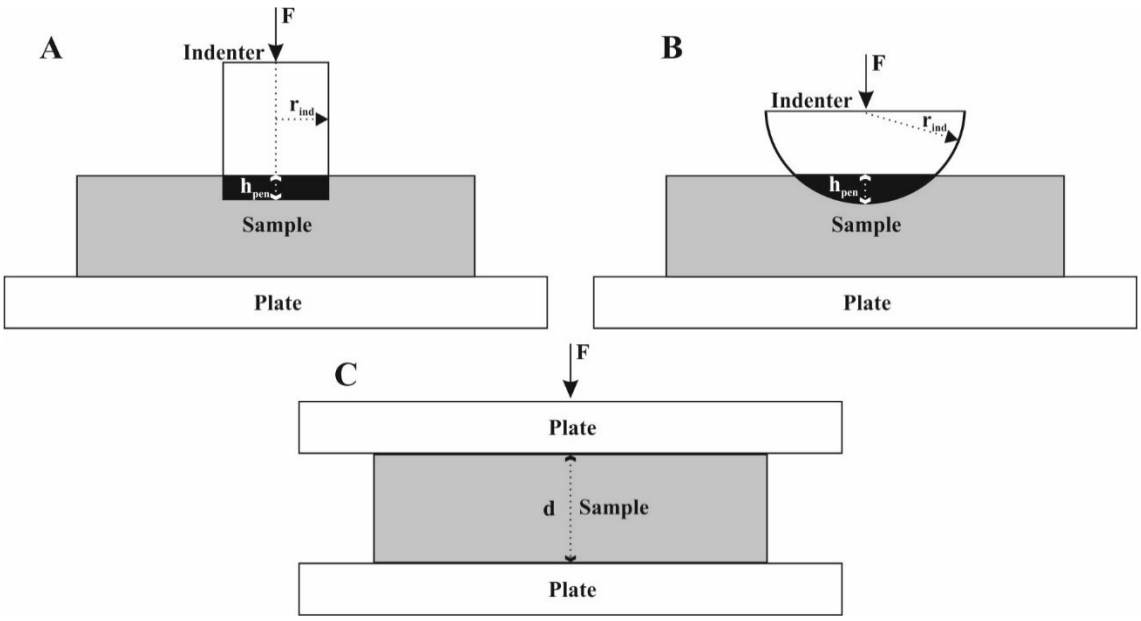

Figure 21 Experimental methods for the viscosity measurements using TMA - A) Penetration method with a cylindrical indenter, B) Penetration method with a hemispherical indenter and C) Parallel-plate setup

Viscosity measurements in melts

Pressure Assisted Melt Filling Technique (PAMFT)

Due to the volatility and corrosivity of chalcogenide melts, the measurement of viscosity in these materials is very complicated and very often these data are missing for the melt region. During the last decade a very skillful technique was developed, the so-called *PAMFT* [143, 144]. This method consists of filling a silica capillary of radius R_C with a molten material by applying a constant pressure *P* as is shown in *Figure 22*.

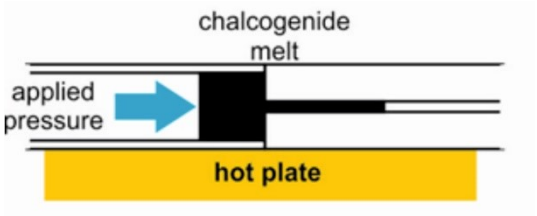

Figure 22 Pressure Assisted Melt Filling Technique (PAMFT)

Since the capillary is positioned horizontally, then the time t dependence of the filling length L is expressed by the equation:

$$L^2 = \left(\frac{P \cdot R_C^2}{4\eta} + \frac{R_C \cdot \gamma \cos\theta}{2\eta}\right) \cdot t \tag{50}$$

However, at certain conditions like high pressure and large capillary radius (i.e., $P \cdot R_C^2 \gg R_C \cdot \gamma \cdot \cos\theta$) *Eq.50* gets simplified into [143]:

$$L^2 = \left(\frac{P \cdot R_C^2}{4\eta}\right) \cdot t \tag{51}$$

Recently, we presented a study of the viscous behavior in *Se*, $Se_{95}Te_5$ and As_2Se_3 melts using the *PAMFT* [145].

Viscosity temperature dependence

Viscosity is a physical parameter with a strong dependence on temperature. One of the most typical equations to describe the temperature dependence of viscosity η is the Arrhenius-type equation:

$$\eta = \eta_0 \cdot exp\left(\frac{E_\eta}{RT}\right) \tag{52}$$

where η_0 is an empirical parameter and E_η corresponds to the apparent activation energy of the viscous flow. However, this equation cannot be used to describe the viscous behavior in fragile glasses like chalcogenide glass-forming materials. In the case of glassy materials, the viscosity is possible to measure from T_g up to T_m. However, the viscosity measurement through the crystallization region is limited. This is one of the reasons why the temperature dependence of the viscosity needs to be extrapolated or interpolated through the crystal growth region. To describe the temperature dependence of viscosity in a wide temperature region for fragile materials, several equations can be used:

Vogel-Fulcher-Tammann (VFT)

$$\log \eta = \log \eta_0 + \frac{B_{VFT}}{(T - T_0)} \qquad \text{[146-148] (53)}$$

Mauro-Yue-Ellison-Gupta-Allan (MYEGA)

$$\log \eta = \log \eta_0 + \frac{K_{MYEGA}}{T} \cdot exp\left(\frac{C_{MYEGA}}{T}\right) \qquad \text{[149] (54)}$$

CHAPTER V:
EXPERIMENTAL PART

Within this thesis the attention is focused on the crystal growth in *Se*, *Se-Te*, and $(GeSe_2)_x(Sb_2Se_3)_{1-x}$ glass-forming materials. The crystal growth is studied by different experimental techniques: microscopy (optical, infrared, scanning electron microscopy-*SEM*) and *DSC*. A suitable combination of these techniques can proffer a deeper perception of the crystal growth mechanism in these materials.

Sample synthesis

The exact amount of pure elements (Sigma Aldrich, 5N) was inserted in a clean silica ampoule. Afterward, the ampoule was evacuated (10^{-4} Pa) and sealed. The samples were prepared by the classic melt-quench technique. The ampoule was then inserted in a furnace and heated to the temperature above T_m for 24 hours. Then the ampoule was cooled down rapidly enough to avoid crystallization. The cooling rate is chosen according to *GFA* of the material. In Table 1, T_m and the cooling media used for the synthesis of the studied glasses are shown.

Table 1 Required parameters for glass synthesis

Glass	***T_m (°C)***	***Cooling medium***
Se	650	Air flow, Water
$Se_{95}Te_5$	650	Air flow, Water
$(GeSe_2)_x(Sb_2Se_3)_{1-x}$	950	Iced water

To study the surface crystal growth in *Se*, $Se_{95}Te_5$ samples, thin films were prepared. To synthesize thin films, the thermal evaporation technique (model UP-858, Tesla Corp.) was used. For example, *Se* thin films were prepared from pure selenium pellets (Sigma Aldrich, 5N) in high vacuum ($2 \cdot 10^{-4}$ Pa). The selenium was deposited on a glass substrate at a deposition rate of 1 – 2 nm. s^{-1}. The substrate was rotated continuously (planetary rotation) to guarantee that the thin film is homogeneous along the whole substrate.

Subsequently, the prepared samples were analyzed by X-Ray diffraction (*XRD*) to verify their amorphous state.

Crystal growth analysis by infrared microscopy

The study of the crystal growth rate was performed both ex-situ and in-situ. In the case of ex-situ experiments, the samples were annealed in a furnace for a certain period of time at a constant temperature (± 1°C). Afterward, the size of the crystals in several samples (up to 5)

was measured using an OLYMPUS BX51 infrared microscope with an integrated OLYMPUS XM10 camera. For in-situ experiments, the samples were annealed on a heating stage (± 0.5°C) (Linkam), which was set within the microscope. In conjunction with the integrated camera was possible to record the crystal growth during the sample's annealing.

The ex-situ experiments were suitable to study the growth rate of a crystalline layer growing towards the core of bulk samples or to study the crystal growth in the inner part of the bulk sample (*volume crystal growth)*. On the other side, in-situ experiments were a suitable tool to measure the crystal growth rate for higher temperatures, where the rate is expected to be high, especially at the surface of bulk samples (*surface growth*).

Crystal growth rate calculation

In-situ experiments

For in-situ experiments, the studied sample was placed into the heating stage and during the sample's annealing the crystal growth was recorded. As is shown in *Figure 23*, the size of individual crystals was measured. Afterward, an l (crystal length) *vs.* t (time) plot was constructed, where the slope of the linear dependence corresponded to the crystal growth rate u. The crystal growth rate was calculated for many crystals (approximately 10 to 15) and the average rate was calculated afterward.

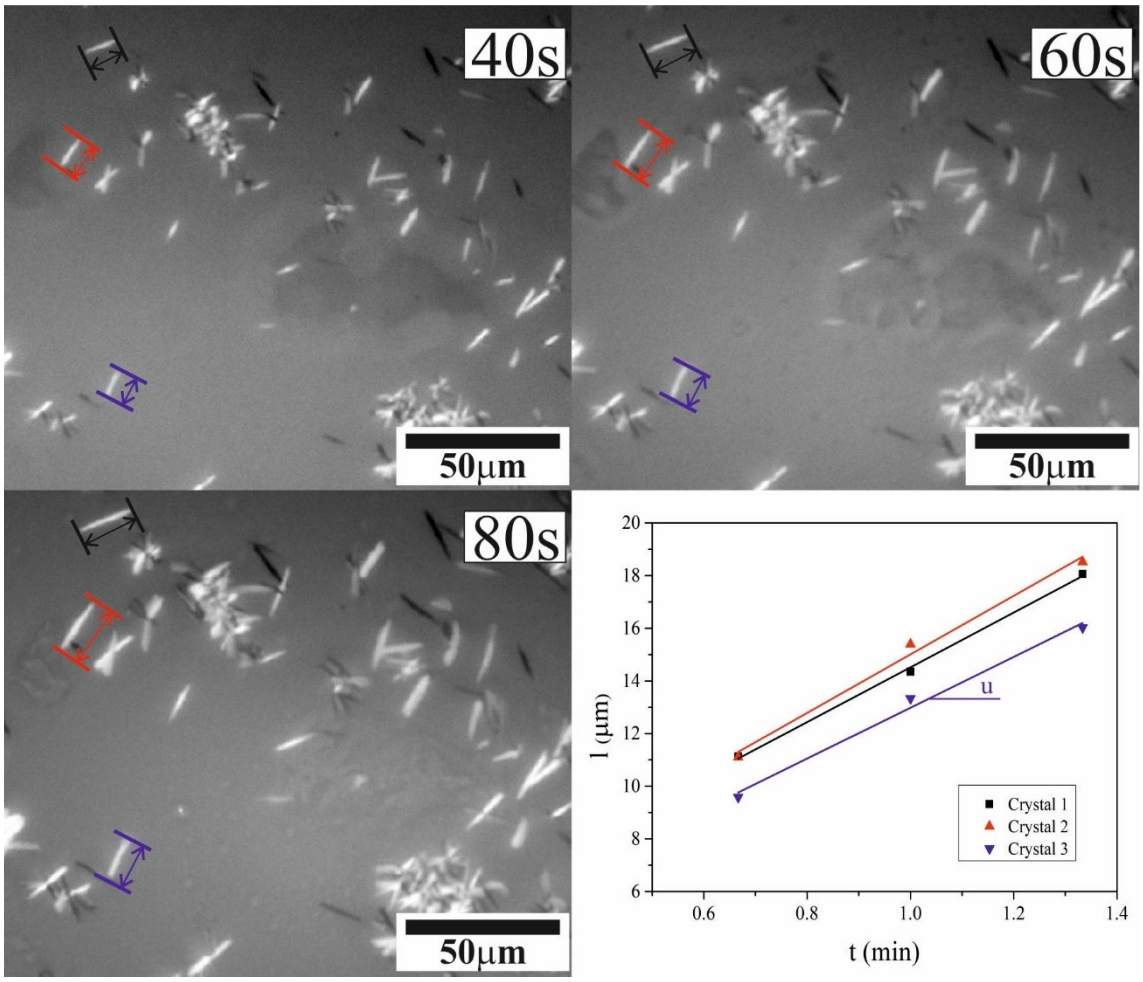

Figure 23 Estimation of the crystal growth rate at the surface of $(GeSe_2)_{0.4}(Sb_2Se_3)_{0.6}$ bulk samples at 335°C studied in-situ.

Ex-situ experiments

Contrary to in-situ experiments, for ex-situ measurements more samples were needed (approximately 3 to 5). This method was used to study the so-called "*volume crystal growth*". Each sample was heated at the same temperature for a different period of time. In the case of $(GeSe_2)_x(Sb_2Se_3)_{1-x}$ bulk samples, the volume crystal growth rate was evaluated from the linear dependence of the measured thickness of the crystalline layer growing towards the core of the sample on time (*Figure 24*). Since the surface of the studied bulk samples was covered by a compact crystalline layer, it was necessary to break and polish the sample in order to observe the crystalline layer growing towards the inner part of the sample.

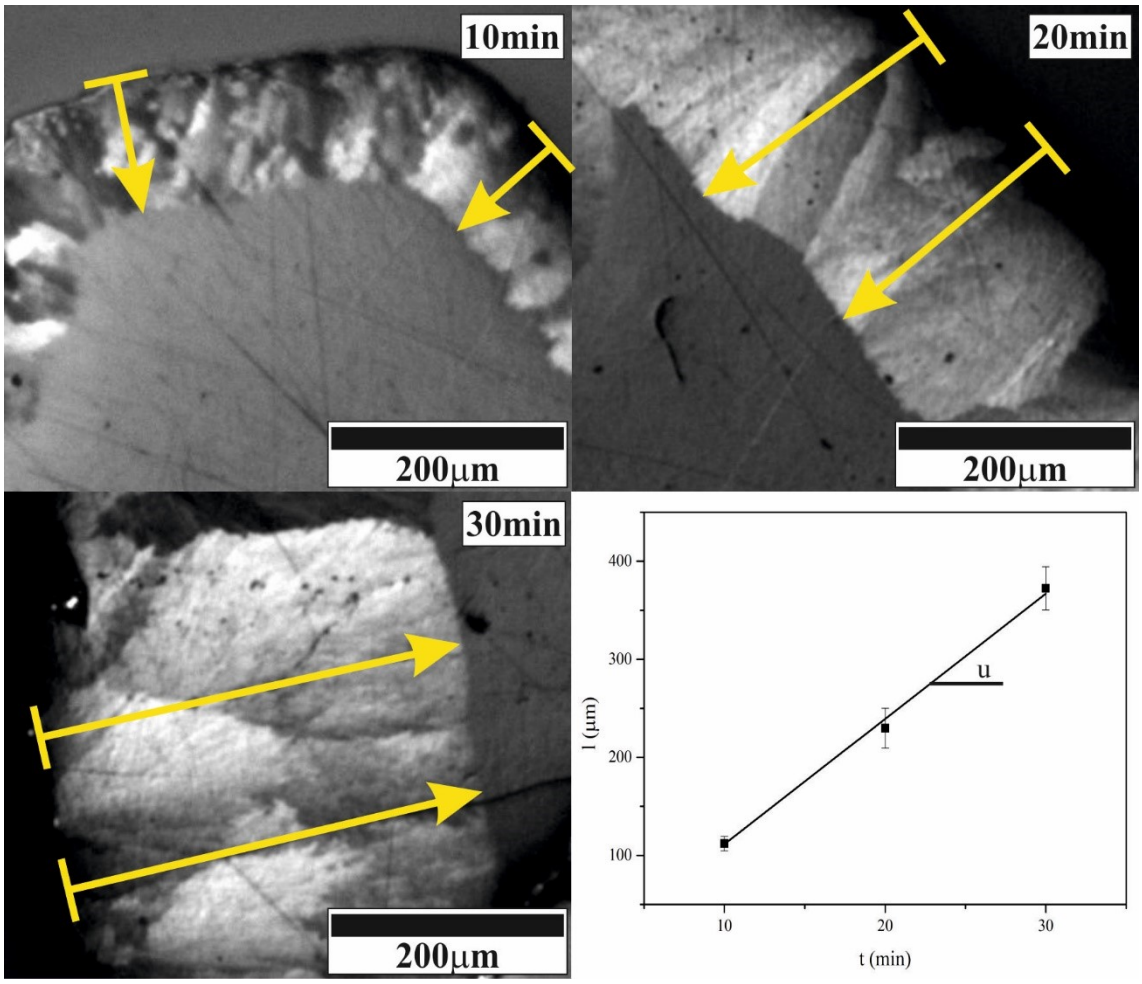

Figure 24 Estimation of the volume crystal growth rate in $(GeSe_2)_{0.4}(Sb_2Se_3)_{0.6}$ bulk samples at 325.3°C studied ex-situ.

Study of crystal growth kinetics by *DSC*

DSC was used to determine valuable parameters such as enthalpy of crystallization ΔH_c, crystallization temperature T_c and melting point T_m. To obtain these values for all the studied materials, the samples were heated in opened silica ampoules (50 – 80 mg in weight) in a *SensysEvo DSC (Seteram Co.)* under non-isothermal conditions at a constant heating rate of 5 $K.min^{-1}$. For illustration purposes, a *DSC* curve for $(GeSe_2)_{0.4}(Sb_2Se_3)_{0.6}$ is shown in *Figure 25*.

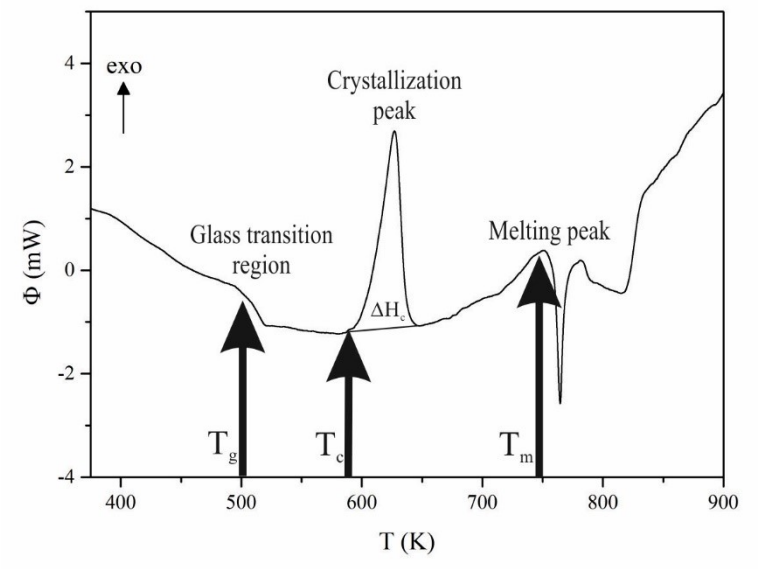

Figure 25 DSC curve of $(GeSe_2)_{0.4}(Sb_2Se_3)_{0.6}$ sample measured under non-isothermal conditions at a heating rate of 5 K.min^{-1}

T_m and T_c values were determined from the onset of the melting and crystallization peak respectively. Enthalpy of crystallization ΔH_c was calculated from the area of the crystallization peak. Before measurements were performed, *DSC* had to be calibrated. This calibration was carried out by measuring the melting of pure metals (Indium, Zinc).

The overall crystallization process in *$GeSe_2$-rich* compositions of the *$(GeSe_2)_x(Sb_2Se_3)_{1-x}$* system (i.e *$x = 0.6 - 0.9$*) was studied using a *DSC Pyris 1 (*Perkin-Elmer co.) calorimeter with an intracooler. The analysis on crystal growth for these compositions was performed for powder samples (20 – 50 μm and 125 – 180 μm). The samples were weighted (ca. 12 mg) into aluminum crucibles without any protective atmosphere, then the crucibles were closed with an aluminum lid. The *DSC* measurements of *$GeSe_2$-rich* compositions (x = 0.6 – 0.9) were performed under non-isothermal conditions. The measurements were performed at several heating rates (0.5, 1, 2, 3, 5, and 10 K.min^{-1}) with a nitrogen flow of 20 ml.min^{-1}. The crystal growth kinetics of *$GeSe_2$-rich* compositions in the *$(GeSe_2)_x(Sb_2Se_3)_{1-x}$* system were analyzed using the software OriTas [150]. Due to the complexity of the studied crystallization process, the *DSC* curves needed to be deconvoluted and several modules of the OriTas software were applied to identify the individual subprocesses (see the *Figure 26* and **Paper V** in the following Chapter VI).

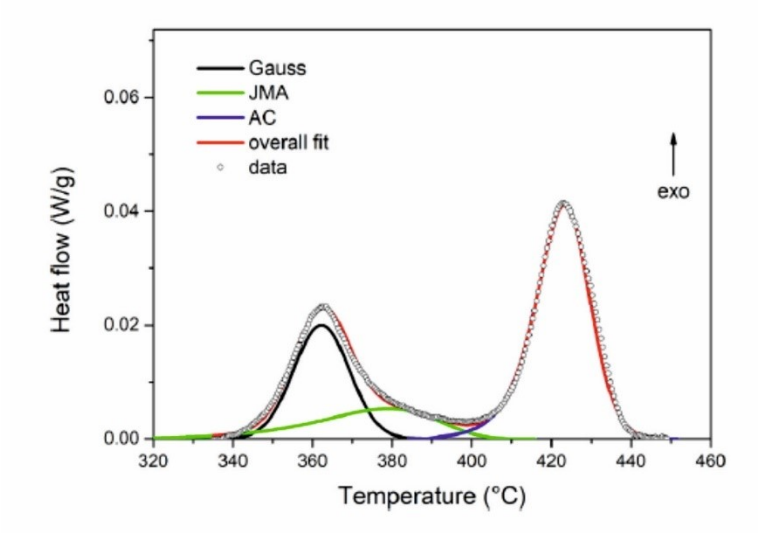

Figure 26 Deconvolution of crystallization peaks in DSC curves for $(GeSe_2)_{0.6}(Sb2se_3)_{0.4}$ sample [151]

Measurement of viscosity

In this thesis the viscosity of $(GeSe_2)_{0.9}(Sb_2Se_3)_{0.1}$ bulk samples were measured in the glass-undercooled melt-melt temperature region. In the case of glass-undercooled melt region, viscosity was measured by thermomechanical analysis. Specifically, thermomechanical analyzers TMA CX03 (RMI – Czech Republic) and TMA PT 1600 (Linseis – Germany). From bulk samples (prepared by the classic melt-quench technique) thin plates with parallel planes were cut into smaller pieces (2.5 mm in height x 6 mm in diameter). The viscosity was measured by penetration method using hemispherical indenter (1.98 mm) and cylindrical indenter (1 mm) in the viscosity range $10^{7.5}$ to $10^{13.5}$. The parallel plate method was used to extend the viscosity measurements to lower viscosity region down to $10^{7.5}$ Pa.s.

Viscosity in the undercooled melt of $Se_{95}Te_5$ thin films was studied following the smoothing process of periodical grating (period 729 nm) embossed into the surface of the prepared amorphous thin film. The embossing process was performed by pressing of master grating onto the surface of the sample at 55 °C (approximately 20 °C above the viscosity glass transition temperature T_{12}). Finally, the samples were heated in a small furnace (temperature stability ± 1°C) and the grating amplitude was characterized by AFM (Multimode8HR, Bruker Nano Inc.).

Viscosity in the melt region for the $Se_{95}Te_5$, using the *PAMFT* technique. To measure the viscosity by *PAMFT* it was necessary to prepare the samples in the form of thin wires. To make such wires, small amount of glassy samples (around 2 g) was introduced into open silica

ampules and melted at 30 °C above melting point in an inert Ar-atmosphere. Using a silica rod, a wire was drawn from the melt by sticking the rod into the melt and pulling it out at a very high speed. For the *PAMFT* measurements, only wires with 60 – 80 μm diameter were selected. *PAMFT* measurements were performed in collaboration with the Institute for Photonic Technologies in Jena, Germany under the supervision of prof. Markus A. Schmidt.

More detail information about the used experimental techniques is presented in Chapter IV.

CHAPTER VI:
SYNOPSIS OF PAPERS

The main goal of this thesis is the kinetic study of crystallization process in amorphous materials. Up to now, there are several discrepancies between the crystal growth mechanism and the contemporary theories about the crystal growth. This is one of the main reasons why the research shown and discussed in this thesis is important. A deep analysis of the crystal growth kinetics in *Se*, $Se_{95}Te_5$ and $(GeSe_2)_x(Sb_2Se_3)_{1-x}$ glasses is presented. The content of this thesis can be summarized in the following points:

- Comparison between volume and surface crystal growth in *Se* and $Se_{95}Te_5$ bulk samples and thin films.
- Comparison between crystal growth at the surface and in the volume of $(GeSe_2)_x(Sb_2Se_3)_{1-x}$ ($x = 0.4 – 0.5$) bulk samples.
- DSC and microscopy study of the complex crystallization process in $GeSe_2$-rich compositions ($x = 0.6 – 0.9$) of $(GeSe_2)_x(Sb_2Se_3)_{1-x}$ glass formers.

Crystal growth kinetics is analyzed from the viewpoint of viscous flow and diffusion. Mainly in this thesis the crystal growth is studied by the combination of *DSC* and Microscopy techniques. Specifically, in this thesis the attention is focused on the variations of the crystal growth kinetics for different compositions and types of samples.

Paper summary I

The first part is focused on the extensive study on crystal growth in different samples of amorphous *Se* (**Paper I**) and $Se_{95}Te_5$ (**Paper II**), which is supported with viscosity measurements in $Se_{95}Te_5$ melts (**Paper III**). Together these works bring a new insight into the competing volume and surface crystal growth with respect to the viscosity and surface diffusion in *Se* and $Se_{95}Te_5$ glass formers.

The aim of the study presented in **Paper I** was to compare the crystal growth rate and mechanism in different types of samples of *a-Se*. In particular, the lateral crystal growth in thin films of different thicknesses (0.2, 1 and 2 μm) and at the surface of bulk samples was compared. The crystals in thin films grew as spherulitic-like structures. In thin films of 0.2 μm thickness another growth mechanism was observed. As is presented in **Paper I**, *SEM* images revealed the formation of some specific crystalline structures, which could be the so-called trigonal selenium flakes [152]. In the case of the crystal growth at the surface of bulk samples, the growth mechanism at the first stage of the crystallization process was different than the one observed in thin films. The crystals at the surface grew as sheaf-like structures, then these structures start branching and the crystals formed into spherulitic-like structures. This growth mechanism was earlier presented by Bisault et al. [153]. The crystal growth rate for both types of samples was calculated. According to these experiments, the crystal growth rates were comparable within the experimental errors. The crystal growth rate in both types of samples was faster than the crystal growth rate in the volume of bulk samples presented in previous studies [46, 100]. The crystal growth rate in thin films is affected by the thickness of the studied samples. For example, the crystal growth in thin films of thickness 200 nm occurs by lower rates than in thin films of 1 μm, 2 μm and at the surface of bulk samples as can be observed in *Figure 27*.

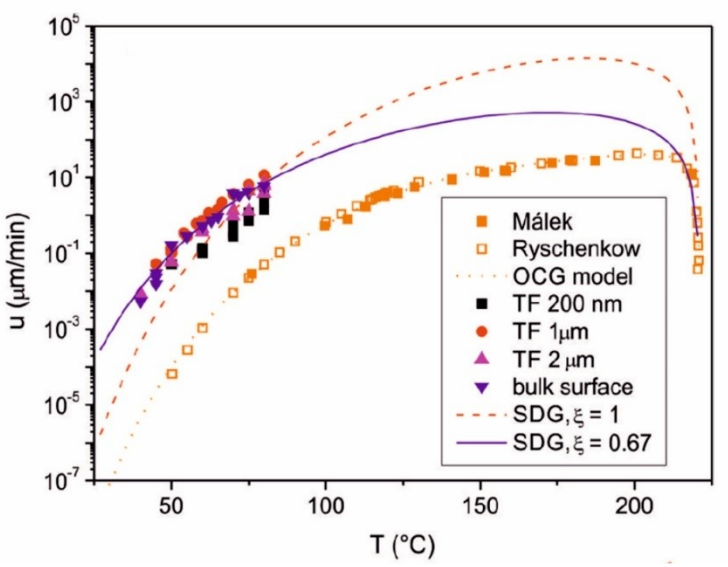

Figure 27 Temperature dependence of the crystal growth rate in Selenium samples [47]

During the characterization of the crystal growth mechanism for a wide temperature range, another important fact was observed. Crystal growth kinetics was characterized by the relation proposed by Ediger et al. [91] ($D(T) \approx u_{kin}(T) \approx \eta(T)^{-\xi}$), which gives a better description of *SE*. The ξ parameter takes values from 0 to 1. When ξ has a value close to 1, it means that the crystal growth kinetics is driven by the viscous flow as is stated by *SE*. This is the case for crystal growth in the volume of *Se* bulk samples, studied by Málek et al. [100] where $\xi = 0.94 \pm 0.05$. On the other hand, the crystal growth mechanism in thin films and at the surface of bulk samples presented a strong decoupling of *SE* ($\xi = 0.67 \pm 0.03$) (*Figure 28*). This is linked to the fact that structural units in thin films and at the surface of bulk samples have a different mobility than in the volume of bulk samples. Then it was possible to state that the crystal growth kinetics in thin films and at the surface of bulk samples is controlled by the surface diffusion rather than by the viscous flow, which is confirmed in the recent work of Barták et al. [133].

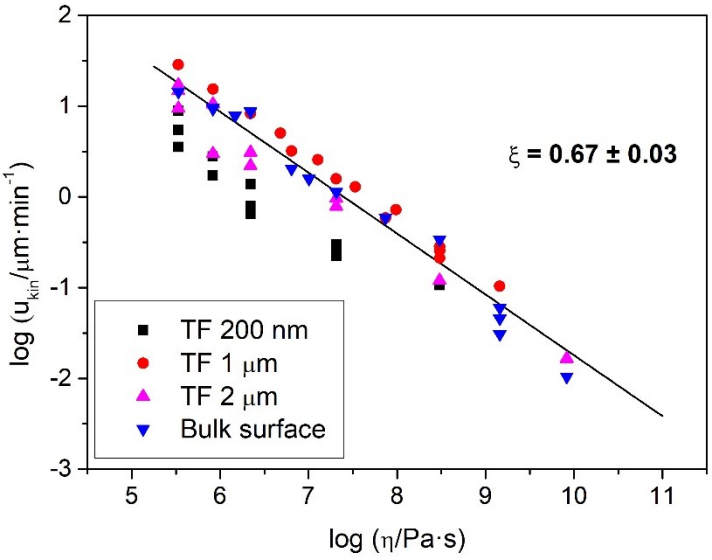

Figure 28 log u_{kin} vs. log η plot for the calculation of ξ [47]

To have a deeper grasp of the relation between the crystal growth rate and the mobility of structural units through the liquid-crystal interface, further research was performed. This study is presented in **Paper II**, which summarizes an extended study on the crystal growth mechanism in $Se_{95}Te_5$ thin films and bulk samples. As was mentioned in **Paper I,** the crystal growth kinetics in thin films and at the surface of bulk samples is different from the growth kinetics in the volume of bulk samples.

In comparison with previous studies in *Se* and *Se-Te* glass formers [59, 100, 154], a different crystal growth mechanism was observed in the volume of $Se_{95}Te_5$ bulk samples. So far it was observed in the *Se-Te* system that the spherulitic-like crystals that grew at the surface formed a compact crystalline layer, which grew towards the core of the sample afterwards. On the other hand, towards the inner part of $Se_{95}Te_5$ samples, a crystalline layer with a diffusive character (i.e., the crystalline layer was not compact) was observed. This impeded the calculation of the crystal growth rate of this crystalline layer. This diffusive behavior was linked to several facts. The diffusive character could have been caused by a faster nucleation process along the vicinity of the surface than in its core, or, by the intrusion of some fiber-like crystals, which grew among the crystalline layer towards the inner part of the sample. Then it is possible to state that this crystal growth mechanism was influenced by a higher mobility in the vicinity of the surface. For this reason, the volume crystal growth rate was estimated by measuring the diameter of the fiber-like crystals and its change in time. A comparable behavior was also observed in organic glassy materials [155]. On the other hand, the crystal growth mechanism in $Se_{95}Te_5$ thin films is comparable to the crystal growth mechanism at the surface of *Se* bulk

samples (**Paper I**). For $Se_{95}Te_5$ thin films, the crystal growth process was followed even below T_g as is presented in **Paper II**. However, at this point an increase in the crystal growth rate was observed. This could be caused by a different growth mechanism comparable with the so-called Glass-Crystal (*GC*) mode, which describes a shift from diffusion-controlled to diffusionless growth [156].

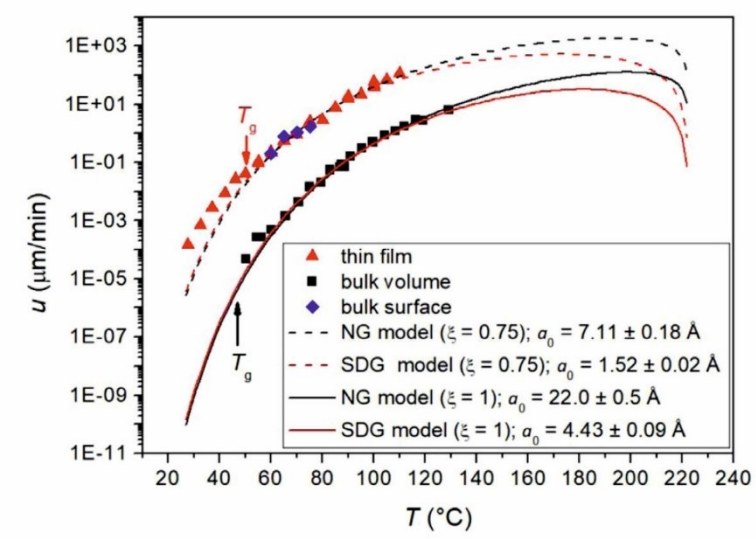

Figure 29 Comparison of crystal growth rates in $Se_{95}Te_5$ samples [122]

As it was presented in **Paper I**, the crystal growth kinetics was described by *SE* relation. In **Paper II**, decoupling of *SE* equation was observed ($\xi = 0.75 \pm 0.02$). Specifically, for crystal growth in thin films and at the surface of bulk samples. Similarly, as it was shown in **Paper I** the crystal growth kinetics were described by the relation proposed by Ediger et al. [91] ($D(T) \approx u_{kin}(T) \approx \eta(T)^{-\xi}$). This relation allowed calculating the correcting parameter ξ. As it is obvious from the relation proposed by Ediger et al. [91], it is necessary to know the temperature dependence of viscosity in these materials. The temperature dependence of $Se_{95}Te_5$ was possible to describe thanks to previous studies on the viscous behavior in supercooled melts [157, 158] and melts. The viscous behavior of $Se_{95}Te_5$ melts was studied using the *Pressure Assisted Melt Filling Technique* (*PAMFT,* **Paper III**). Based on the study presented in **Paper III**, *PAMFT* can be considered as a very useful technique for the determination of viscosity in chalcogenide materials. Measuring at high pressure, the volatility of chalcogenide materials is suppressed. Another significant advantage of this technique is the small amount of sample that is needed. In **Paper II**, the viscous behavior in $Se_{95}Te_5$ thin films and at the surface of bulk samples was studied. According to findings presented in **Paper II**, it is possible to state that viscous flow in thin films and bulk samples is equivalent. With the knowledge of the viscosity temperature dependence, the decoupling parameter could be calculated. For the volume crystal growth

kinetics, $\xi = 0.97$ was calculated, which confirms that the volume mobility of structural units can be expressed by *SE* equation using the inverse viscosity. On the other hand, for the crystal growth in thin films and at the surface of bulk samples, the value of $\xi = 0.75$ was calculated. However, as it is presented in **Paper II,** for temperatures below T_g, the correcting parameter ξ decreased to 0.52. This remarkable decrease of ξ value confirms a change in the crystal growth mechanism, which leads to the increase in the crystal growth rate for temperatures below T_g as is shown in *Figure 29.*

In **Paper II**, the apparent activation energy of the surface diffusion and the viscous flow were calculated to compare both processes. For this purpose, it was necessary to find the temperature dependence of the surface diffusion coefficient. The surface diffusion coefficients were estimated using the power relation: $u_s \approx D_s^{0.87}$. This relation was known for organic glass-formers [127] and recently the same relation was confirmed also for *a-Se* [133]. Then, after calculating the activation energies of both surface diffusion and viscous flow, it was confirmed that the surface diffusion in $Se_{95}Te_5$ had a lower activation energy than the viscous flow, which corresponds to the higher mobility of structural units along the surface resulting in faster crystal growth there than the in the volume.

Paper summary II

The second part of paper conclusions is dedicated to the crystal growth in $(GeSe_2)_x(Sb_2Se_3)_{1-x}$ glass-formers. **Paper IV** presents a direct study of the crystal growth kinetics in the $(GeSe_2)_x(Sb_2Se_3)_{1-x}$ system (where $x = 0.4$ *and* 0.5) and its relation to the viscous flow and diffusion. **Paper V** shows a complex *DSC* analysis of the crystallization process in $GeSe_2$-rich compositions ($x = 0.6 – 0.9$). **Paper VI** is focused on the direct observation of the crystal growth process of Sb_2Se_3 and $GeSe_2$ crystals using microscopy techniques.

The crystal growth process in this glass-forming system is very complex and it was necessary to perform a deep analysis on it, as is shown in **Paper IV, Paper V** and **Paper VI**.

A detailed analysis of the overall nucleation-growth process in these materials is presented in **Paper V**. Previously, several *DSC* analyses of $(GeSe_2)_x(Sb_2Se_3)_{1-x}$ ($x = 0.3 – 0.5$) glass-forming materials were performed by Svoboda [8, 10]. For these compositions, only one crystallization peak was observed under both isothermal and non-isothermal conditions. Where the crystallization process corresponded to Sb_2Se_3 crystalline phase [8, 10, 68, 72]. On the other hand, for $GeSe_2$*-rich* compositions, *DSC* measurements presented in **Paper V** revealed a

complex crystallization process (*Figure 30*), which corresponds to the growth of individual crystalline phases (Sb_2Se_3 and $GeSe_2$). Due to the very complex crystallization behavior which took place in the entire region between glass transition and eutectic melting, the *DSC* measurements were performed at very slow heating rates (from 0.5 $K.min^{-1}$ to 10 $K.min^{-1}$) to split up several individual kinetic processes and subsequently analyze the complex crystallization process before T_m was reached. In the case of bulk samples, the crystallization process was very slow, and it was interrupted by the eutectic melting before it was completed, even at low heating rates. According to the study presented in **Paper IV** and that published by Svoboda [10], crystal growth of Sb_2Se_3 at the surface of bulk samples and in powder samples ($x = 0.3 – 0.5$) was observed at lower temperatures. This shift is related to the fact that with decreasing particle size, the surface area of the samples increases, providing a larger area for the crystal growth occurring before the eutectic melting occurs. For this reason, the study of the crystallization process presented in **Paper V** was performed only in powder samples, with particle size of 20-50μm and 125-180μm. The kinetic analysis was performed using OriTas software [150], which uses the classical kinetic equations (*JMA, AC*) to calculate and estimate the most suitable model that can describe the experimental data.

As is shown in *Figure 30*, for the $x = 0.6$ composition (*Figure 30 (A)*), two crystallization peaks were observed. The first peak corresponds to Sb_2Se_3 crystalline phase and the second peak corresponds to $GeSe_2$ crystalline phase. With increasing x (i.e., increasing $GeSe_2$ content), Sb_2Se_3 crystallization peak decreases and a clear detachment from the $GeSe_2$ crystallization peak is no longer observed. This is the case for $x = 0.7$ and 0.8 (*Figure 30(B)* and *(C)* respectively) compositions. In the case of ($x = 0.9$) composition, *DSC* measurements showed that crystallization process started at a temperature above T_g and presented a very complicated character, which was not complete within the analyzed temperature range. For this reason, *DSC* scans of $x = 0.9$ composition were not subjected to kinetic analysis (see **Paper V**).

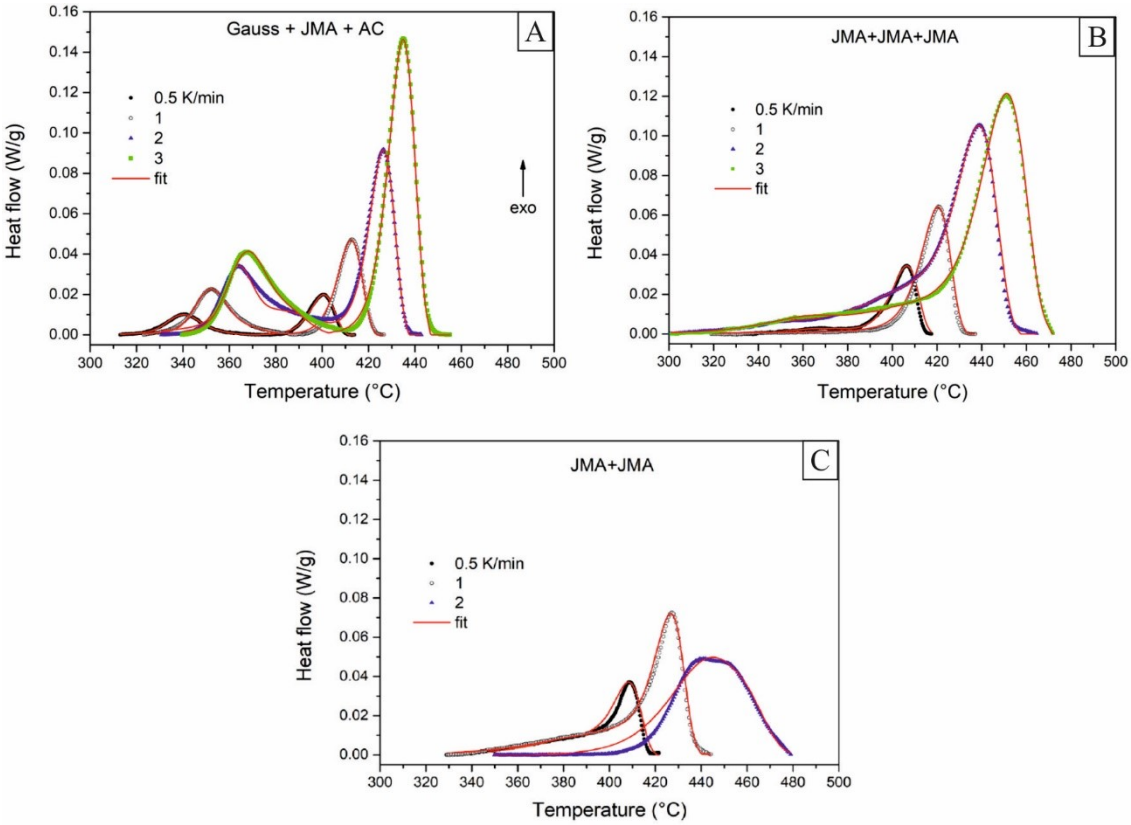

Figure 30 DSC crystallization peaks for A) $(GeSe_2)_{0.6}(Sb_2Se_3)_{0.4}$, B) $(GeSe_2)_{0.7}(Sb_2Se_3)_{0.3}$ and C) $(GeSe_2)_{0.8}(Sb_2Se_3)_{0.2}$ powder samples with a particle size of 20-50 μm [151].

Continuing with the kinetic analysis of the crystal growth in $(GeSe_2)_x(Sb_2Se_3)_{1-x}$ glass-forming materials, **Paper IV** and **Paper VI (Draft)** present a detailed analysis using microscopy techniques. The main goal in **Paper IV** was to explain observed differences in the crystal growth mechanism at the surface and in the volume of $(GeSe_2)_x(Sb_2Se_3)_{1-x}$ (for $x = 0.4$ *and* 0.5) bulk samples. At the surface of bulk samples, the so-called lateral growth was observed. At the beginning of the crystal growth at the surface, Sb_2Se_3 crystals grew from thin needles and continued branching, as it was observed in previous studies [159]. Since Sb_2Se_3 crystals had uniform sizes, it is suitable to state that the nucleation process in this system took place quickly and was finished before the crystal growth took place. Due to the high density of nuclei at the surface of the samples, a compact crystalline layer was formed. This layer continued growing from the surface towards the core of the studied samples. This growth mechanism was denoted in **Paper IV** as "volume crystal growth". Apart from this compact layer, another type of crystal was observed. In the core of the studied samples, some spherical-like crystals were formed. This type of crystal was denoted in **Paper IV** as "competing volume crystals". The denominated "competing volume crystals" grew separately from the compact crystalline layer. However, it is important to mention that the radius of the so-called "competing

volume crystals" and the thickness of the compact crystalline layer grew at the same rate. Then, in **Paper IV** both types of crystal growth are considered as volume crystal growth. Both, surface and volume, crystal growth mechanisms were observed in both $(GeSe_2)_{0.4}(Sb_2Se_3)_{0.6}$ and $(GeSe_2)_{0.5}(Sb_2Se_3)_{0.5}$ compositions. In the case of $(GeSe_2)_{0.6}(Sb_2Se_3)_{0.4}$ samples, although Sb_2Se_3 crystallization process is significant (as shown in *DSC* scans in **Paper V**), no compact crystalline layer was observed (see *Figure 31*). For this reason, the kinetic study of the volume crystal growth was performed only in $(GeSe_2)_{0.4}(Sb_2Se_3)_{0.6}$ and $(GeSe_2)_{0.5}(Sb_2Se_3)_{0.5}$ compositions (**Paper IV**).

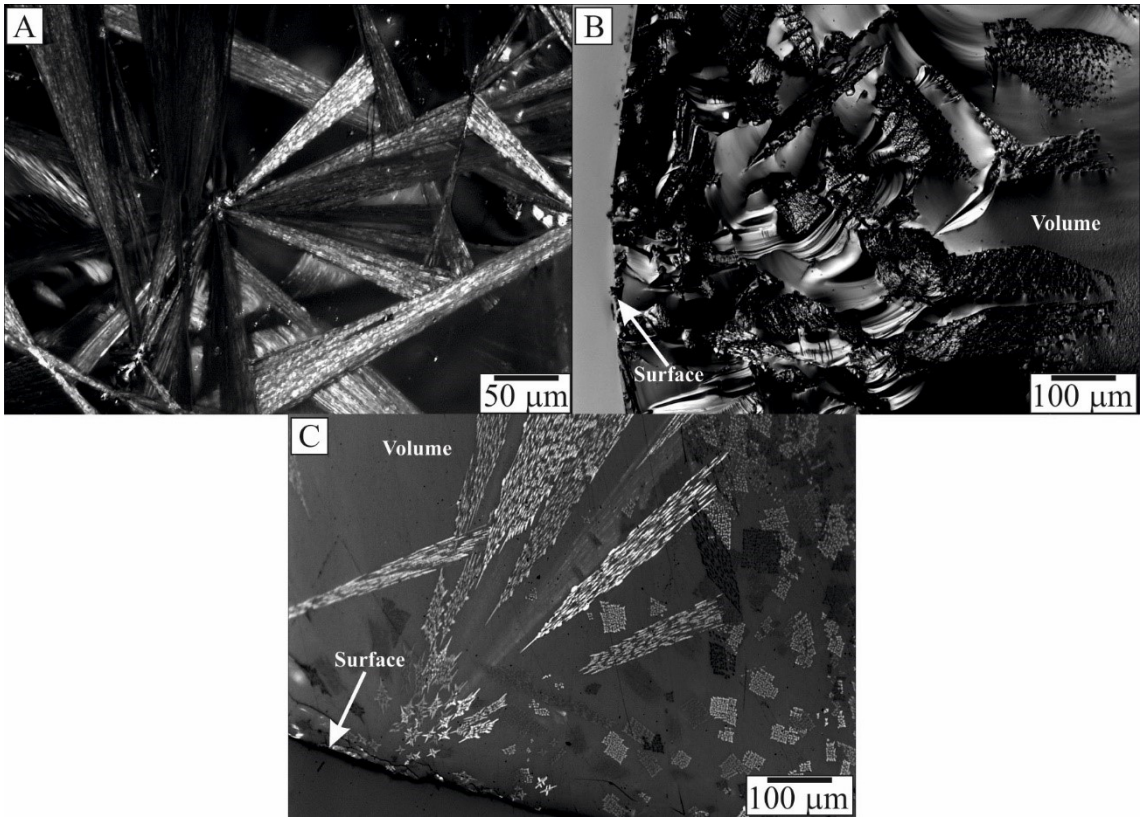

Figure 31 Infrared micrographs of Sb_2Se_3 crystals in $(GeSe_2)_{0.6}(Sb_2Se_3)_{0.4}$ bulk samples- A) Fully crystallized surface, B) Fracture and C) Polished sample

It is important to mention that with increasing Sb_2Se_3 content, the crystal growth rate is increased (i.e., the crystal growth rate reaches higher values at lower temperatures). Essentially, for both compositions ($x = 0.4$ and 0.5) the activation energy for surface crystal growth is lower than that for volume crystal growth. In **Paper IV**, a comparison between the activation energy values obtained by Svoboda [10] from *DSC* measurements and the activation energy values obtained from microscopy measurements revealed an important fact. For $x = 0.4$, the activation energy published by Svoboda [10] is comparable with the activation energy of the volume crystal growth. This phenomenon might be linked with the fact, that for composition $x = 0.4$

the volume crystal growth is dominant in the overall crystallization process. On the other hand, for $x = 0.5$, the activation energy published by Svoboda [10] is similar to the activation energy of the surface crystal growth. This suggests that the overall crystallization process corresponds to the surface crystal growth. This information can be provided only by the direct observation of the crystal growth using microscopy techniques. However, microscopy measurements have limitations such as the inability to observe the crystal growth at high rates. For this reason, it is necessary to estimate the behavior of the crystal growth for a wide temperature range, using the well-known *NG* and *SDG* crystal growth models. In the case of the surface lateral crystal growth, a crucial phenomenon was revealed. A deviation of the experimental data from the calculated crystal growth models (*NG* and *SDG*) was observed. According to several studies presented previously [47, 160-162], this is related to the decoupling from *SE* equation, which describes the relationship between the crystal growth kinetics and the viscosity. The decoupling from the *SE* equation is mostly related to the competition of several factors such as: volume diffusion, surface self-diffusion and the surface tension. For this reason, the relation between the crystal growth kinetics and the viscosity was analyzed by the relation proposed by Ediger et al. [91]. Then, the decoupling parameter ξ was calculated for $(GeSe_2)_{0.4}(Sb_2Se_3)_{0.6}$ (ξ =0.7), $(GeSe_2)_{0.5}(Sb_2Se_3)_{0.5}$ (ξ = 0.74) and $(GeSe_2)_{0.6}(Sb_2Se_3)_{0.4}$ (ξ = 0.77) compositions (**Paper VI**). From this data is evident that with decreasing Sb_2Se_3 content, ξ finds higher values. It is then possible to state that for lower Sb_2Se_3 content, the crystal growth kinetics are more influenced by the volume diffusion (i.e., ξ values closer to 1). On the other hand, for the volume crystal growth in $x = 0.4$ and 0.5 compositions, it was concluded that the kinetic barrier and the transport of structural units from the melt to the crystal-liquid interface is driven by the volume diffusion, since for $x = 0.4$ and $x = 0.5$ compositions the decoupling parameter ξ = 0.92 was calculated. Therefore, it is feasible to state that the volume crystal growth kinetics for both $x = 0.4$ and $x = 0.5$ compositions, can be described using viscosity data according to the *SE*.

In **Paper VI (Draft)** the crystal growth in $(GeSe_2)_x(Sb_2Se_3)_{1-x}$ (where $x = 0.6 – 0.9$) glass-formers was analyzed at the surface of bulk samples. As it was presented in **Paper V**, for $(GeSe_2)_{0.6}(Sb_2Se_3)_{0.4}$ samples, the crystallization process of Sb_2Se_3 and $GeSe_2$ phases occurred. Since Sb_2Se_3 crystal growth started earlier (i.e., at lower temperatures) than the crystal growth of $GeSe_2$, at the moment when $GeSe_2$ crystallization started, the surface was full of Sb_2Se_3 crystals and it was therefore impossible to observe $GeSe_2$ crystals using microscopy techniques. The presence of $GeSe_2$ crystalline phase was, however confirmed by *XRD* analysis (**Paper V**). For $x = 0.7$ and 0.8 compositions, both Sb_2Se_3 and $GeSe_2$ crystalline phases were observed as

was discerned from *DSC* scans in **Paper V**. Apart from the *DSC* scans, both Sb_2Se_3 and $GeSe_2$ crystals were observed in $x = 0.7$ and 0.8 compositions using microscopy techniques (**Paper V**). However, it is important to remark that these crystals were formed under non-isothermal conditions. From non-isothermal experiments it was impossible to estimate the crystal growth rate of both phases growing simultaneously. While studying the crystal growth kinetics in these compositions ($x = 0.7$ and 0.8) (**Paper VI (Draft)**) under isothermal conditions, another crucial phenomenon was observed. As is shown in *Figure 32*, at the early stage of the isothermal treatment, Sb_2Se_3 crystals are larger than $GeSe_2$ crystals. However, during the heat treatment of the sample, Sb_2Se_3 crystals became smaller while $GeSe_2$ crystals became bigger with time (it seems that Sb_2Se_3 crystals melted or dissolved after the crystal growth of $GeSe_2$ was enhanced). For this reason, it was impossible to calculate the crystal growth rate of Sb_2Se_3 at temperatures where the crystallization process of $GeSe_2$ was predominant. In the case of $(GeSe_2)_{0.9}(Sb_2Se_3)_{0.1}$ samples, Sb_2Se_3 crystal growth was totally suppressed and only $GeSe_2$ crystals were observed.

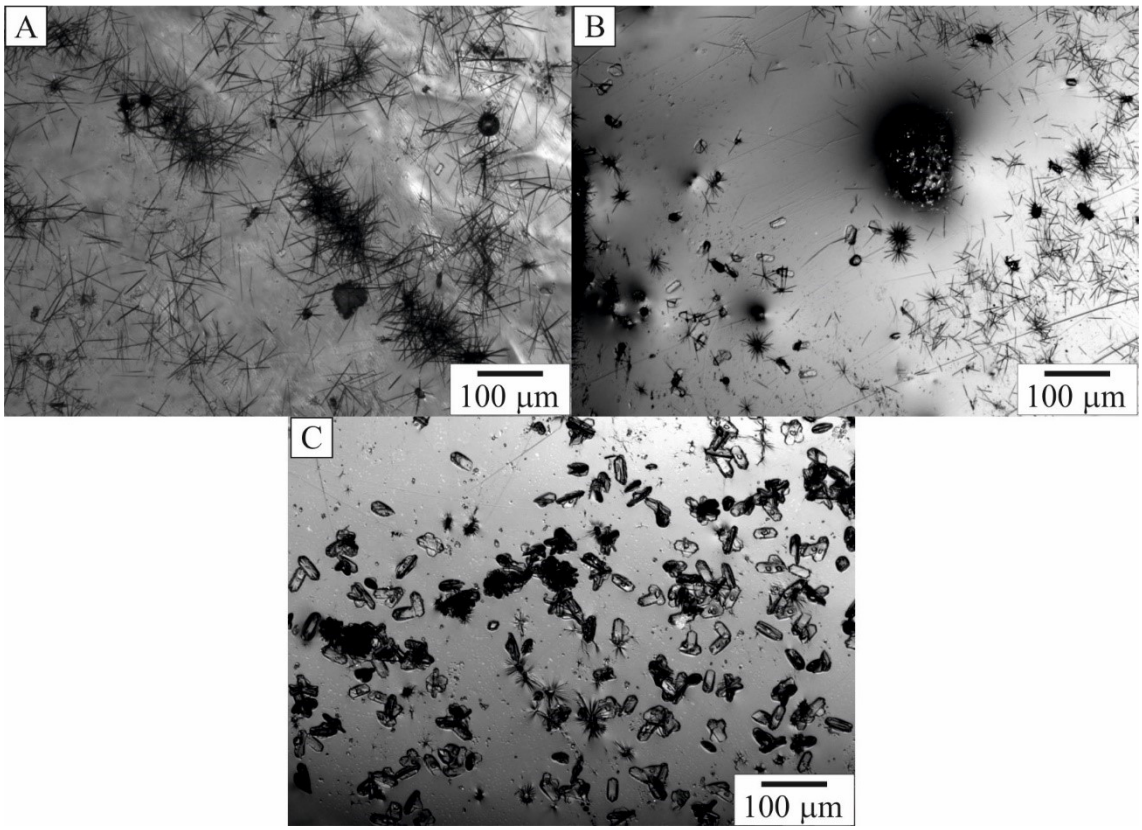

Figure 32 Sb_2Se_3 (needles) and $GeSe_2$ (tetragonal structures) crystals growing under isothermal conditions at T =687.8 K, A) t =20 min, B) t = 30 min, C) t = 40 min at the surface of $(GeSe_2)_{0.7}(Sb_2Se_3)_{0.3}$ bulk samples.

$GeSe_2$ growth kinetics also presented a decoupling from the *SE* relation, where ξ decreased with increasing $GeSe_2$ content. However, for $GeSe_2$ phase, the decrease of ξ is more abrupt than for Sb_2Se_3.

CONCLUSIONS

Since the stability of chalcogenide glass-forming materials represent a very important ally in the development of technological devices, the main intention of this doctoral thesis was to give a deeper grasp on the crystal growth kinetics of such materials. Crystallization kinetics were studied using several experimental techniques such as: Microscopy techniques (*IR, SEM*), Thermal analysis (*DSC, TMA*) and *XRD.* The experimental results were analyzed within the contemporary crystal growth theories and compared with previous studies published in scientific literature. The experimental results presented in this thesis were divided in two parts. The first part was dedicated to the analysis of the crystal growth in *Se* and $Se_{95}Te_5$ samples. The second part focused on the crystal growth kinetics in $(GeSe_2)_x(Sb_2Se_3)_{1-x}$ pseudobinary system. The main outcomes are presented as follows.

Part I

Se

- The crystal growth in thin films and at the surface of bulk was compared under isothermal conditions.
- Similar crystal morphology was observed in thin films and at the surface of bulk samples. Since such crystals grew linearly within time, it was confirmed that the crystal growth is ruled by the liquid-melt interface kinetics.
- The crystal growth rate in thin films and at the surface of bulk samples was compared with volume crystal growth rate. The crystal growth behavior for a wide temperature range in such samples was estimated by contemporary growth models (*NG* and *SDG*)
- Crystal growth kinetics in thin films and at the surface of bulk samples presented a strong decoupling of the *SE* relation. It was demonstrated that this might be linked to the fact that the crystal growth kinetics in such samples is driven by surface diffusion rather than by viscous flow.
- It was demonstrated that *Pressure Assisted Melt Filling Technique* - *PAMFT* can be used to study the viscous behavior of chalcogenide materials in the melt region.

$Se_{95}Te_5$

- The crystal growth kinetics in thin films, at the surface and towards the volume of bulk samples, and its relation to the mobility of structural units from the amorphous to the crystalline phase, was analyzed.
- The volume crystal growth in bulk samples, revealed formation of fiber-like crystalline structures which differ from the crystals observed in other *Se-Te* compositions.
- The crystal growth in thin films was observed even at temperatures below T_g, where an interesting growth mechanism was revealed. A significant decoupling between surface crystal growth rate and viscosity was observed. According to the obtained results, this is linked to the fast crystal growth driven by a high surface mobility. Considering this fact, the crystal growth behavior of such samples was estimated for a wide temperature range using crystal growth models, which consider the effect of viscosity and surface diffusion.

Part II

$(GeSe_2)_x(Sb_2Se_3)_{1-x}$

- Indirect *DSC* study of crystallization process was complemented with direct microscopy techniques.
- The crystal growth mechanism was studied at the surface and in the volume of bulk samples. Several compositions were analyzed (i.e., from $x = 0.4$ to $x = 0.9$)
- In the case of $x = 0.4$ and $x = 0.5$ compositions, the crystal growth was studied at the surface and towards the volume of bulk samples. Two types of crystal growth mechanisms were observed.
- The surface crystal growth kinetics of both Sb_2Se_3 and $GeSe_2$ phases in all the compositions, presented a strong decoupling from the *SE* relation. This phenomenon might be linked to the fact that the surface crystal growth kinetics of both crystalline phases are driven by the surface diffusion rather than viscous flow. On the other hand, for volume crystal growth, no decoupling was observed.
- In the case of $GeSe_2$-*rich* compositions ($x = 0.6 – 0.9$), *DSC* scans revealed that the crystallization of Sb_2Se_3 was followed by $GeSe_2$. Both types of crystalline structures were identified by *XRD* and the crystal growth mechanism was analyzed by microscopy techniques.

Although, crystallization have been studied for many decades, this thesis gave a very complex view of the crystal growth behavior in chalcogenide glass-forming materials. First, this thesis presented a comparison between surface and volume crystal growth mechanisms. The crystal growth was analyzed in several types of samples such as thin films, powder and bulk samples. Combining various experimental methods (microscopy, *DSC*, *TMA*, *XRD*), important information about the crystallization process in the studied samples was obtained. From this obtained information was possible to estimate the crystal growth behavior in several chalcogenide glass-forming materials for a wide temperature range.

The second aim of this thesis was to understand and compare processes such as viscosity and diffusion, which are responsible for transport of structural units from undercooled melt to crystalline phase. For this study, growth rate and viscosity data were needed. Data revealed that the crystal growth kinetics can be driven by viscous flow mostly in the volume of bulk samples, by diffusion mostly on surface of bulk samples and in thin films, or, as was shown for crystal growth observed in $Se_{95}Te_5$ below T_g, by other mechanism.

In some cases, the crystallization process should be avoided as is the case for solar panels and optical fibers. On the other hand, there are technological materials which need the crystallization to occur as is the case for *PCM*. The results presented in this doctoral thesis offer comprehensive information about the thermal behavior of such glass formers, which might be very useful in improving the quality of established technologies and for the development of new technological devices.

REFERENCES

1. Zhou, Y., et al., *Solution-Processed Antimony Selenide Heterojunction Solar Cells.* Adv. Energy Mater., 2014. **4**(8).
2. Huang, F.Q., C.Y. Yang, and D.Y. Wan, *Advanced solar materials for thin-film photovoltaic cells.* Front. Phys., 2011. **6**(2): p. 177-196.
3. Lyubin, V., *Chalcogenide glassy photoresists: History of development, properties, and applications.* Phys. Status Solidi B-Basic Solid State Phys., 2009. **246**(8): p. 1758-1767.
4. Raoux, S., et al., *Phase change materials and phase change memory.* MRS Bull., 2014. **39**(8): p. 703-710.
5. Afonso, C.N., et al., *Ultrafast Reversible Phase-Change in GeSb films for erasable optical storage.* Appl. Phys. Lett., 1992. **60**(25): p. 3123-3125.
6. Ohno, E., et al., *TeGeSnAu Alloys for Phase-Change type of Optical Disk Memories.* Japan. J. Appl. Phys. Part 1 - Regul. Pap. Short Notes Rev. Pap., 1989. **28**(7): p. 1235-1240.
7. Lee, J.H., et al., *Crystallization behavior of Ge-Sb-Se glasses in the compositional range for use as molded lenses.* J. Non Cryst. Solids, 2018. **481**: p. 21-26.
8. Svoboda, R., *Crystallization of $(GeSe_2)_{0.3}(Sb_2Se_3)_{0.7}$ chalcogenide glass-Influence of reaction atmosphere.* J. Non Cryst. Solids, 2019. **509**: p. 23-30.
9. Svoboda, R., J. Gutwirth, and J. Malek, *Crystallization kinetics of a-Se, part 4: thin films.* Philosophical Magazine, 2014. **94**(26): p. 3036-3051.
10. Svoboda, R., *Oxidation-influenced crystallization in $(GeSe_2)_x(Sb_2Se_3)_{1-x}$ chalcogenide glasses.* J. Non Cryst. Solids, 2019. **510**: p. 6-14.
11. Malek, J., et al., *Crystallization kinetics of $Ge_{0.3}Sb_{1.4}S_{2.7}$ glass.* Thermochim. Acta, 1996. **280**: p. 353-361.
12. Horst, S., *Glass: Nature, Structure, and Properties*, 1991, Springer Science & Business Media.
13. Debenedetti, P.G. and F.H. Stillinger, *Supercooled liquids and the glass transition.* Nature, 2001. **410**(6825): p. 259-267.
14. Queiroz, C.A. and J. Šesták, *Aspects of the non-crystalline state.* Phys. Chem. Glasses-Eur. J. GlassSci. Technol. Part B, 2010. **51**(3): p. 165-172.
15. Ediger, M.D., C.A. Angell, and S.R. Nagel, *Supercooled liquids and glasses.* J. Phys. Chem., 1996. **100**(31): p. 13200-13212.
16. Zanotto, E.D. and J.C. Mauro, *The glassy state of matter: Its definition and ultimate fate.* J. Non Cryst. Solids, 2017. **471**: p. 490-495.
17. Zachariasen, W.H., *The atomic arrangement in glass.* J. Am. Chem. Soc., 1932. **54**(10): p. 3841-3851.
18. Montazerian, M. and E.D. Zanotto, *The Glassy State.* Reference Module in Materials Science and Materials Engineering, 2019.
19. Jiang, Z.H. and Q.Y. Zhang, *The structure of glass: A phase equilibrium diagram approach.* Prog. Mater. Sci., 2014. **61**: p. 144-215.
20. Hruby, A., *Evaluation of Glass-Forming Tendency by Means of DTA.* Czech. J. Phys. Sect. B, 1972. **B 22**(11): p. 1187-&.
21. Moreno, T.V., et al., *Potentiometric sensors with chalcogenide glasses as sensitive membranes: A short review.* J. Non Cryst. Solids, 2018. **495**: p. 8-18.
22. Vassilev, V. and S. Boycheva, *Chemical sensors with chalcogenide glassy membranes.* Talanta, 2005. **67**(1): p. 20-27.
23. Mehta, N., *Applications of chalcogenide glasses in electronics and optoelectronics: A review.* J. Sci. Ind. Res., 2006. **65**(10): p. 777-786.
24. Parnell, H., et al., *Compositional dependence of crystallization in Ge–Sb–Se glasses relevant to optical fiber making.* J. Am. Ceram. Soc., 2018. **101**(1): p. 208-219.
25. Wuttig, M. and N. Yamada, *Phase-change materials for rewriteable data storage.* Nat. Mater., 2007. **6**(11): p. 824-832.
26. Raoux, S., W. Wełnic, and D. Ielmini, *Phase change materials and their application to nonvolatile memories.* Chem. Rev., 2010. **110**(1): p. 240-267.

27. Ma, H.L., X.H. Zhang, and J. Lucas, *Infrared transmitting chalcogenide glass ceramics.* J. Non Cryst. Solids, 2003. **317**(3): p. 270-274.
28. Wronski, M.M., et al., *A solid-state amorphous selenium avalanche technology for low photon flux imaging applications.* Med. Phys., 2010. **37**(9): p. 4982-4985.
29. Guisbiers, G., et al., *Anti-bacterial selenium nanoparticles produced by UV/VIS/NIR pulsed nanosecond laser ablation in liquids.* Laser Phys. Lett., 2015. **12**(1).
30. Guisbiers, G., et al., *Inhibition of E. coli and S. aureus with selenium nanoparticles synthesized by pulsed laser ablation in deionized water.* Int. J. Nanomed., 2016. **11**: p. 3731.
31. Lara, H.H., et al., *Synergistic antifungal effect of chitosan-stabilized selenium nanoparticles synthesized by pulsed laser ablation in liquids against Candida albicans biofilms.* Int. J. Nanomed., 2018. **13**: p. 2697-2708.
32. Tan, H.W., et al., *Selenium Species: Current Status and Potentials in Cancer Prevention and Therapy.* Int. J. Mol. Sci., 2019. **20**(1).
33. Hosnedlova, B., et al., *Nano-selenium and its nanomedicine applications: a critical review.* Int. J. Nanomed., 2018. **13**: p. 2107-2128.
34. Bubon, O., et al., *Amorphous selenium (a-Se) avalanche photosensor with metal electrodes.* J. Non Cryst. Solids, 2012. **358**(17): p. 2431-2433.
35. Bubon, O., et al., *Electroded avalanche amorphous selenium (a-Se) photosensor.* Curr. Appl. Phys., 2012. **12**(3): p. 983-988.
36. Zhou, X.M., et al., *Amorphous, Crystalline and Crystalline/Amorphous Selenium Nanowires and Their Different (De)Lithiation Mechanisms.* Chem. Mat., 2015. **27**(19): p. 6730-6736.
37. Li, J., et al., *Facile synthesis of hollow carbonized polyaniline spheres to encapsulate selenium for advanced rechargeable lithium-selenium batteries.* J. Alloy. Compd., 2015. **619**: p. 794-799.
38. Panahi-Kalamuei, M., M. Salavati-Niasari, and S.M. Hosseinpour-Mashkani, *Facile microwave synthesis, characterization, and solar cell application of selenium nanoparticles.* J. Alloy. Compd., 2014. **617**: p. 627-632.
39. Abbaszadeh, S., et al., *Application of organic semiconductors in amorphous selenium based photodetectors for high performance X-ray imaging*, in *Medical Imaging 2013: Physics of Medical Imaging*, R.M. Nishikawa, B.R. Whiting, and C. Hoeschen, Editors. 2013, Spie-Int Soc Optical Engineering: Bellingham.
40. Niu, Y.S., et al., *Biocompatible Single-Crystal Selenium Nanobelt Based Nanodevice as a Temperature-Tunable Photosensor.* J. Nanomater., 2012. **2012**.
41. Li, Y.Z., et al., *A Monolithic Amorphous-Selenium/CMOS Visible-Light Imager With Sub-9-mu m Pixel Pitch and Extended Full-Well Capacity.* IEEE Sens. J., 2021. **21**(1): p. 339-346.
42. Pal, S.K., et al., *Some novel results of physical aging studies in glassy selenium.* Mater. Sci. Eng. B-Adv. Funct. Solid-State Mater., 2020. **259**.
43. Zhang, H.Y., Z.Q. Hu, and K. Lu, *Transformation from The Amorphous to The Nanocrystalline State in Pure Selenium.* Nanostruct. Mater., 1995. **5**(1): p. 41-52.
44. Mikla, V.I., et al., *Molecular structure of Se-rich amorphous films.* Prog. Solid State Chem., 2018. **49**: p. 1-15.
45. Málek, J. and R. Svoboda, *Kinetic Processes in Amorphous Materials Revealed by Thermal Analysis: Application to Glassy Selenium.* Molecules, 2019. **24**(15): p. 2725.
46. Ryschenkow, G. and G. Faivre, *Bulk Crystallization of Liquid Selenium - Primary Nucleation, Growth-Kinetics and Modes of Crystallization.* J. Cryst. Growth, 1988. **87**(2-3): p. 221-235.
47. Bartak, J., et al., *Comparison of Lateral Crystal Growth in Selenium Thin Films and Surface of Bulk Samples.* Cryst. Growth Des., 2018. **18**(7): p. 4103-4110.
48. Metzger, W., et al., *Recombination kinetics and stability in polycrystalline Cu(In, Ga)Se_2 solar cells.* Thin Solid Films, 2009. **517**(7): p. 2360-2364.
49. Wu, X.Z., *High-efficiency polycrystalline CdTe thin-film solar cells.* Sol. Energy, 2004. **77**(6): p. 803-814.
50. Fiducia, T.A.M., et al., *Understanding the role of selenium in defect passivation for highly efficient selenium-alloyed cadmium telluride solar cells.* Nat. Energy, 2019. **4**(6): p. 504-511.
51. Bureau, B., et al., *Tellurium based glasses: A ruthless glass to crystal competition.* Solid State Sci., 2008. **10**(4): p. 427-433.

52. Zhang, X., H. Ma, and J. Lucas, *Applications of chalcogenide glass bulks and fibres.* Journal of Optoelectronics and Advanced Materials, 2003. **5**(5): p. 1327-1333.
53. Svoboda, R., M. Kincl, and J. Malek, *Thermal characterization of Se-Te thin films.* J. Alloy. Compd., 2015. **644**: p. 40-46.
54. Geoffrion, L.D. and G. Guisbiers, *Physico-chemical properties of selenium-tellurium alloys across the scales.* Nanoscale Adv.
55. Mendoza-Galvan, A., et al., *Structural, optical and electrical characterization of amorphous Se_xTe_{1-x} thin film alloys.* Microelectron. Eng., 2000. **51-2**: p. 677-687.
56. Khan, Z.H., et al., *Electrical and optical properties of a-Se_xTe_{100-x} thin films.* Opt. Laser Technol., 2012. **44**(1): p. 6-11.
57. Mauro, J.C. and A.K. Varshneya, *Modeling of selenium telluride glass.* Phys. Status Solidi B-Basic Solid State Phys., 2005. **242**(6): p. R46-R48.
58. Svoboda, R., M. Krbal, and J. Malek, *Crystallization kinetics in Se-Te glassy system.* J. Non Cryst. Solids, 2011. **357**(16-17): p. 3123-3129.
59. Bartak, J., S. Martinkova, and J. Malek, *Crystal growth kinetics in Se–Te bulk glasses.* Cryst. Growth Des., 2015. **15**(9): p. 4287-4295.
60. Martinková, S., et al., *Crystal growth in $Se_{70}Te_{30}$ thin films followed by SEM and in situ XRD.* J. Appl. Phys., 2016. **120**(14): p. 145301.
61. Klocek, P., M. Roth, and R. Rock, *Chalcogenide glass optical fibers and image bundles: properties and applications.* Opt. Eng., 1987. **26**(2): p. 260288.
62. Baudet, E., et al., *Infrared sensor for water pollution and monitoring*, in *Optical Sensors 2017*, F. Baldini, J. Homola, and R.A. Lieberman, Editors. 2017, Spie-Int Soc Optical Engineering: Bellingham.
63. Zhang, X.H., et al., *Enhancement of charge photo-generation and transport via an internal network of Sb_2Se_3/Cu_2GeSe_3 heterojunctions.* J. Mater. Chem. A, 2014. **2**(40): p. 17099-17106.
64. Xu, Y., et al., *Enhanced conductivity and photoelectric performance of $GeSe_2$–Sb_2Se_3-based glass ceramics by CuI doping.* J. Mater. Sci. Mater. Electron., 2020. **31**(2): p. 1654-1660.
65. Xu, Y., et al., *Crystallization optimization of the $40GeSe_2$-$40Sb_2Se_3$-20CuI glass for improvement of photoelectric properties.* J. Non Cryst. Solids, 2016. **431**: p. 61-67.
66. Senapati, U. and A.K. Varshneya, *Viscosity of chalcogenide glass-forming liquids: An anomaly in the 'strong' and 'fragile' classification.* J. Non Cryst. Solids, 1996. **197**(2-3): p. 210-218.
67. Mahadevan, S., et al., *Dilatometric studies on Ge-Sb-Se glasses.* J. Non Cryst. Solids, 1984. **65**(2-3): p. 233-240.
68. Wei, W.H., et al., *Crystallization kinetics and thermal stability in Ge–Sb–Se glasses.* Phys. Status Solidi B, 2013. **250**(1): p. 59-64.
69. Sharma, N., et al., *Effect of antimony addition on thermal stability and crystallization kinetics of germanium-selenium alloys.* J. Non Cryst. Solids, 2013. **371**: p. 1-5.
70. Sharma, N., et al. *Structural Rigidity, Percolation and Transition-Temperature Study of the $Ge_{19}Se_{81-x}Sb_x$ System*. in *Defect and Diffusion Forum*. 2011. Trans Tech Publ.
71. Lee, W.H., et al., *Thermal expansion behavior of Ge-Sb-Se glasses in a compositional range for molded infrared lens applications.* Int. J. Appl. Glass Sci., 2017. **8**(2): p. 226-232.
72. Bordas, S., M.T. Clavagueramora, and N. Clavaguera, *Glass-Formation and Crystallization Kinetics of some Ge-Sb-Se Glasses.* J. Non Cryst. Solids, 1990. **119**(2): p. 232-237.
73. Bordas, S., M.T. Clavagueramora, and B. Legendre, *Phase-Diagram of the Ternary System Ge-Sb-Se.* Thermochim. Acta, 1982. **56**(2): p. 161-182.
74. Sakai, K., et al., *Crystallization of amorphous $GeSe_2$ semiconductor by isothermal annealing without light radiation.* Japan. J. Appl. Phys. Part 1 - Regul. Pap. Short Notes Rev. Pap., 2000. **39**(3A): p. 1058-1061.
75. Inoue, K., O. Matsuda, and K. Murase, *Raman-Spectra of Tetrahedral Vibrations in Crystalline Germanium Dichalcogenides, GeS_2 and $GeSe_2$, In High and Low-temperature forms.* Solid State Commun., 1991. **79**(11): p. 905-910.
76. Nakaoka, T., et al., *Trifurcated crystallization and inhomogeneity in $GeSe_2$ glass.* Phys. Rev. B, 2001. **63**(22).
77. Voutsas, G.P., et al., *The Crystal-Structure of Antimony Selenide, Sb_2Se_3.* Z. Kristall., 1985. **171**(3-4): p. 261-268.

78. Tideswell, N.W., F.H. Kruse, and J.D. McCullough, *The Crystal Structure of Antimony Selenide, Sb_2Se_3.* Acta Crystallogr., 1957. **10**(2): p. 99-102.
79. Savory, C. and D.O. Scanlon, *The complex defect chemistry of antimony selenide.* J. Mater. Chem. A, 2019. **7**(17): p. 10739-10744.
80. Fokin, V.M., et al., *Homogeneous crystal nucleation in silicate glasses: a 40 years perspective.* J. Non Cryst. Solids, 2006. **352**(26-27): p. 2681-2714.
81. Rao, K., *Structural chemistry of glasses*2002: Elsevier.
82. Uhlmann, D. and B. Chalmers, *The energetics of nucleation.* Ind. Eng. Chem., 1965. **57**(9): p. 19-31.
83. Schmelzer, J.W. and A.S. Abyzov, *Crystallization of glass-forming liquids: Thermodynamic driving force.* J. Non Cryst. Solids, 2016. **449**: p. 41-49.
84. Kelton, K.F., *Crystal Nucleation in Liquids and Glasses.* Solid State Phys., 1991. **45**: p. 75-177.
85. Markov, I.V., *Crystal Growth for Beginners: Fundamentals of Nucleation, Crystal Growth and Epitaxy*, 2003, World Scientific.
86. Kirkpatrick, R.J., *Crystal growth from the melt: a review.* Am. Mineral.:J. Earth Planet. Mater., 1975. **60**(9-10): p. 798-814.
87. Christian, J.W., *The Theory of Transformations in Metals and Alloys* 1965: Pergamon Press,Oxford.
88. Christen.Nh, A.R. Cooper, and B.S. Rawal, *Kinetics of Dendritic Precipitation of Cristobalite from a Potassium Silicate Melt* J. Am. Ceram. Soc., 1973. **56**(11): p. 557-561.
89. Elbaum, C., *Substructures in Crystals Grown from the Melt.* Progress in Metal Physics, 1959. **8**: p. 203-&.
90. Hopper, R.W. and D.R. Uhlmann, *Temperature Distributions during Crystallization at Constant Velocity.* J. Cryst. Growth, 1973. **19**(3): p. 177-186.
91. Ediger, M., P. Harrowell, and L. Yu, *Crystal growth kinetics exhibit a fragility-dependent decoupling from viscosity.* J. Chem. Phys., 2008. **128**(3): p. 034709.
92. Nascimento, M.L.F., E.B. Ferreira, and E.D. Zanotto, *Kinetics and mechanisms of crystal growth and diffusion in a glass-forming liquid.* J. Chem. Phys., 2004. **121**(18): p. 8924-8928.
93. Podzemna, V., J. Bartak, and J. Malek, *Crystal growth kinetics in GeS_2 amorphous thin films.* J. Therm. Anal. Calorim., 2014. **118**(2): p. 775-781.
94. Uhlmann, D.R., *Crystal growth in glass forming system*, in *Advances in Nucleation and Crystallization in Glasses*, L.L. Hench and S.W. Freiman, Editors. 1972, American Ceramics Society: Ohio. p. 91-115.
95. Burgner, L.L. and M.C. Weinberg, *Crystal growth mechanisms in inorganic glasses.* Phys. Chem. Glasses, 2001. **42**(3): p. 184-190.
96. Jackson, K., *Current concepts in crystal growth from the melt.* Prog. Solid State Chem., 1967. **4**: p. 53-80.
97. Hillig, W.B. and D. Turnbull, *Theory of Crystal Growth in Undercooled Pure Liquids.* J.Chem. Phys., 1956. **24**(4): p. 914-914.
98. Jackson, K., D.R. Uhlmann, and J. Hunt, *On the nature of crystal growth from the melt.* J. Cryst. Growth, 1967. **1**(1): p. 1-36.
99. Kaldis, E. and H.J. Scheel, *Current Topics in Materials Science*1977: North-Holland Publishing Company.
100. Malek, J., J. Bartak, and J. Shanelova, *Spherulitic Crystal Growth Velocity in Selenium Supercooled Liquid.* Cryst. Growth Des., 2016. **16**(10): p. 5811-5821.
101. Thompson, C.V. and F. Spaepen, *Approximation of The Free-Energy Change on Crystallization.* Acta Metall., 1979. **27**(12): p. 1855-1859.
102. Singh, H.B. and A. Holz, *Stability Limit of Supercooled Liquids.* Solid State Commun., 1983. **45**(11): p. 985-988.
103. Hoffman, J.D., *Thermodynamic Driving Force in Nucleation and Growth Processes.* J.Chem. Phys., 1958. **29**(5): p. 1192-1193.
104. Turnbull, D., *Formation of crystal nuclei in liquid metals.* J. Appl. Phys., 1950. **21**(10): p. 1022-1028.
105. Avrami, M., *Kinetics of phase change. I General theory.* J. Chem. Phys., 1939. **7**(12): p. 1103-1112.

106. Henderson, D.W., *Thermal-Analysis of Nonisothermal Crystallization Kinetics in Glass Forming Liquids.* J. Non Cryst. Solids, 1979. **30**(3): p. 301-315.
107. Yinnon, H. and D.R. Uhlmann, *Applications of thermoanalytical techniques to the study of crystallization kinetics in glass-forming liquids, part I: theory.* J. Non Cryst. Solids, 1983. **54**(3): p. 253-275.
108. Šesták, J. and G. Berggren, *Study of the kinetics of the mechanism of solid-state reactions at increasing temperatures.* Thermochim. Acta, 1971. **3**(1): p. 1-12.
109. Sestak, J. and J. Malek, *Diagnostic Limits of Phenomenological Models of Heterogeneous Reactions and Thermal-Analysis Kinetics.* Solid State Ion., 1993. **63-5**: p. 245-254.
110. Malek, J., *Kinetic analysis of crystallization processes in amorphous materials.* Thermochim. Acta, 2000. **355**(1-2): p. 239-253.
111. Kissinger, H.E., *Reaction Kinetics in Differential Thermal Analysis.* Anal. Chem., 1957. **29**(11): p. 1702-1706.
112. Kissinger, H.E., *Variation of Peak Temperature with Heating Rate in Differential Thermal Analysis.* J. Res. Natl. Bur. Stand., 1956. **57**(4): p. 217-221.
113. Ozawa, T., *Kinetic analysis of derivative curves in thermal analysis.* J. Therm. Anal., 1970. **2**(3): p. 301-324.
114. Friedman, H.L., *New Methods for Evaluating Kinetic Parameters from Thermal Analysis Data.* J. Polym. Sci. Pol. Lett., 1969. **7**(1PB): p. 41-&.
115. Stevenson, J.D. and P.G. Wolynes, *On the surface of glasses.* J.Chem. Phys., 2008. **129**(23).
116. Daley, C., et al., *Comparing surface and bulk flow of a molecular glass former.* Soft Matter, 2012. **8**(7): p. 2206-2212.
117. Yang, Z.H., et al., *Glass Transition Dynamics and Surface Layer Mobility in Unentangled Polystyrene Films.* Science, 2010. **328**(5986): p. 1676-1679.
118. de Gennes, P.G., *Glass transitions in thin polymer films.* Eur. Phys. J. E, 2000. **2**(3): p. 201-203.
119. Fakhraai, Z. and J.A. Forrest, *Measuring the surface dynamics of glassy polymers.* Science, 2008. **319**(5863): p. 600-604.
120. Zhu, L., et al., *Surface Self-Diffusion of an Organic Glass.* Phys. Rev. Lett., 2011. **106**(25).
121. Ruan, S., et al., *Surface diffusion and surface crystal growth of tris-naphthyl benzene glasses.* J.Chem. Phys., 2016. **145**(6).
122. Martinková, S., et al., *Relationship between crystal growth and surface/volume mobilities in $Se_{95}Te_5$ bulk glasses and thin films.* Acta. Mater., 2021: p. 116953.
123. Cao, C.R., et al., *High surface mobility and fast surface enhanced crystallization of metallic glass.* Appl. Phys. Lett., 2015. **107**(14).
124. Cao, C.P., L. Yu, and J.H. Perepezko, *Surface dynamics measurement on a gold based metallic glass.* Appl. Phys. Lett., 2020. **116**(23).
125. Zhang, W. and L. Yu, *Surface Diffusion of Polymer Glasses.* Macromolecules, 2016. **49**(2): p. 731-735.
126. Hasebe, M., et al., *Fast Surface Crystal Growth on Molecular Glasses and Its Termination by the Onset of Fluidity.* J. Phys. Chem. B, 2014. **118**(27): p. 7638-7646.
127. Huang, C.B., et al., *Fast Surface Diffusion and Crystallization of Amorphous Griseofulvin.* J. Phys. Chem. B, 2017. **121**(40): p. 9463-9468.
128. Schmalzried, H., *Solid state reactions*1974: Verlag chemie.
129. Mehrer, H., *Diffusion in intermetallics.* Mater. Trans. JIM, 1996. **37**(6): p. 1259-1280.
130. Faupel, F., et al., *Diffusion in metallic glasses and supercooled melts.* Rev. Mod. Phys., 2003. **75**(1): p. 237-280.
131. Mehrer, H. *Diffusion in Glassy Metals*. in *Diffusion Foundations*. 2014. Trans Tech Publ.
132. Mullins, W.W., *Flattening of a Nearly Plane Solid Surface due to Capillarity.* J. Appl. Phys., 1959. **30**(1): p. 77-83.
133. Barták, J., et al., *Mobility in Amorphous Selenium and Comparison with Organic Molecular Glasses.* J.Chem. Phys., 2021. **154**(7).
134. Koštál, P., J. Shánělová, and J. Málek, *Viscosity of chalcogenide glass-formers.* Int. Mater. Rev., 2020. **65**(2): p. 63-101.
135. Yang, F.Q. and J.C.M. Li, *Newtonian viscosity measured by impression test.* J. Non Cryst. Solids, 1997. **212**(2-3): p. 126-135.

136. Koštál, P., T. Hofírek, and J. Málek, *Viscosity measurement by thermomechanical analyzer.* J. Non Cryst. Solids, 2018. **480**: p. 118-122.
137. Exnar, P., et al., *Experience with The Penetration Viscosimeter.* Silikaty, 1980. **24**(2): p. 169-179.
138. Douglas, R.W., et al., *A Penetration Viscometer* Glass Technol., 1965. **6**(2): p. 52-55.
139. Koštál, P. and J. Málek, *Viscosity of $(GeSe_2)_x(Sb_2Se_3)_{1-x}$ undercooled melts.* J. Non Cryst. Solids, 2007. **353**(29): p. 2803-2806.
140. Fontana, E.H., *A Versatille Parallel-Plate Viscometer for Glass Viscosity Measurements to 1000 Degrees C.* Am. Ceram. Soc. Bull., 1970. **49**(6): p. 594-597.
141. Gent, A.N., *Theory of The Parallel Plate Viscometer.* Brit. J. Appl. Phys., 1960. **11**(2): p. 85-87.
142. Chromcikova, M. and P. Dej, *Structural relaxation of NBS711 glass - Reliability of the regression estimates of relaxation model.* Ceram.-Silik., 2006. **50**(3): p. 125-129.
143. Wang, S.Y., et al., *Non-Newtonian flow of an ultralow-melting chalcogenide liquid in strongly confined geometry.* Appl. Phys. Lett., 2015. **106**(20).
144. Da, N., et al., *High index-contrast all-solid photonic crystal fibers by pressure-assisted melt infiltration of silica matrices.* J. Non Cryst. Solids, 2010. **356**(35-36): p. 1829-1836.
145. Barták, J., et al., *Analysis of viscosity data in As_2Se_3, Se and $Se_{95}Te_5$ chalcogenide melts using the pressure assisted melt filling technique.* J. Non Cryst. Solids, 2019. **511**: p. 100-108.
146. Fulcher, G.S., *Analysis of Recent Measurements of the Viscosity of Glasses - Reprint.* J. Am. Ceram. Soc., 1992. **75**(5): p. 1043-1059.
147. Tammann, G. and W. Hesse, *Die Abhängigkeit der Viscosität von der Temperatur bie unterkühlten Flüssigkeiten.* Z. Anorg. Allg. Chem., 1926. **156**(1): p. 245-257.
148. Vogel, H., Phys. Zeit. 22, 1921: p. 645-646.
149. Mauro, J.C., et al., *Viscosity of glass-forming liquids.* Proc. Natl. Acad. Sci. U. S. A., 2009. **106**(47): p. 19780-19784.
150. Pilný, P. *OriTas Program – Solution for Kinetic Analysis of Thermoanalytical Data*. 2020; Available from: http://www.petrpilny.cz/oritasen.
151. Honcová, P., et al., *Combination of indirect and direct approaches to the description of complex crystallization behavior in $GeSe_2$-rich region of pseudobinary $GeSe_2$–Sb_2Se_3 system.* J. Non Cryst. Solids, 2021. **568**: p. 120968.
152. Suzuki, Y., et al., *Crystalline trigonal selenium flakes grown by vapor deposition and its photodetector application.* Mater. Lett., 2020. **275**.
153. Bisault, J., G. Ryschenkow, and G. Faivre, *Spherulitic Branching in the crystallization of Liquid Selenium.* J. Cryst. Growth, 1991. **110**(4): p. 889-909.
154. Bartak, J., R. Svoboda, and J. Malek, *Electrical conductivity and crystallization kinetics in Te-Se glassy system.* J. Appl. Phys., 2012. **111**(9).
155. Shi, Q. and T. Cai, *Fast Crystal Growth of Amorphous Griseofulvin: Relations between Bulk and Surface Growth Modes.* Cryst. Growth Des., 2016. **16**(6): p. 3279-3286.
156. Sun, Y., et al., *Crystallization near glass transition: Transition from diffusion-controlled to diffusionless crystal growth studied with seven polymorphs.* J. Phys. Chem. B, 2008. **112**(18): p. 5594-5601.
157. Kostal, P. and J. Malek, *Viscosity of selenium melt.* J. Non Cryst. Solids, 2010. **356**(50-51): p. 2803-2806.
158. Koštál, P. and J. Málek, *Viscosity of Se–Te glass-forming system.* Pure Appl. Chem., 2015. **87**(3): p. 239-247.
159. Wang, D., et al., *Growth of one-dimensional Sb_2S_3 and Sb_2Se_3 crystals with straw-tied-like architectures.* J. Cryst. Growth, 2005. **281**(2-4): p. 611-615.
160. Barták, J., et al., *Crystal growth in $(GeS_2)_x(Sb_2S_3)_{1-x}$ thin films.* J. Non Cryst. Solids, 2015. **410**: p. 7-13.
161. Martinková, S., et al., *Extended Study on Crystal Growth and Viscosity in Ge–Sb–Se Bulk Glasses and Thin Films.* J. Phys. Chem. B, 2017. **121**(33): p. 7978-7986.
162. Bartak, J., P. Kostal, and J. Malek, *Analysis of crystal growth and viscosity in Ge-Sb-Se-Te undercooled melts.* J. Non Cryst. Solids, 2019. **505**: p. 1-8.